Non-contact measurement of heart rate using a camera

Albin Berggren, Jenny Berggren

March 1, 2019

LUND
UNIVERSITY

Master's thesis in
Biomedical engineering
Faculty of Engineering LTH
Department of Biomedical Engineering
Supervisor: Frida Sandberg

Abstract

Measurements of heart rate without contact can be of much importance when the possibilities of skin contact for different reasons are limited, or for monitoring at distance over time. This is an emerging area in our time, and the idea to construct a working system to demonstrate the technique was therefore born. The work has been performed at the Department of Biomedical Engineering at LTH.

The main question to answer during the project was whether or not it was possible to construct a real-time working system to perform contact-less measurements of heart rate using a camera. The specifications held on the hardware as well as the developed software and surroundings of the possible measurements have been examined.

Limitations have been made that the subject being under measurement can not move his or her head faced away from the camera. An invariant light intensity in the room has also been assumed, which limits the environments and circumstances under which measurements may be performed.

The results showed the significance of light conditions in the room when performing measurements, as well as of adequate signal processing algorithms to reduce noise and verify the correct heart rate. After tests performed on 9 different subjects in varying environments a mean deviation from the reference of approximately half a beat per minute was obtained. Further tests must be performed in order to conclude what causes this deviation and how it may be solved.

The presented results show that with further testing of different algorithms and environmental factors the proposed technique may be of great importance in measurements of heart rate in the future.

This project has been performed at the Department of Biomedical Engineering at LTH. During the process we have gained much insight in first of all how to implement our combined knowledge from many different areas. It has been very interesting to be able to dig deeper into a current area under development that we both see much potential for in the future. Being able to combine our growing knowledge of the field with the expertise of our supervisor as well as the many scientific articles that has been gone through has been developing and making this work possible. We would therefor like to give many thanks to our supervisor Frida Sandberg for all the support, help and encouragement she has given to us throughout the process.
We would also like to aim a big thank you to the persons that took part in our testing of the program. The time they dedicated to help us with collecting data was a very important part of our project made possible thanks to them.
Last but not least, to everyone around us that has encouraged us during this journey, many heart warm thanks for all the support.
/Albin and Jenny Berggren

Contents

1 Introduction **4**

2 Background **5**
2.1 Heartbeat 5
2.2 PPG 5

3 Theory **7**
3.1 Camera 7
3.2 Lighting conditions 8
3.3 Detection and traction of region of interest 8
3.4 Spatial averaging 11
3.5 Color channel selection 11
3.6 Filtering 13
3.7 Extraction of pulse signal 13
3.8 Welch's method of spectral estimation 14
3.9 Resolution of frequency spectrum 15
3.10 Statistical analysis 15

4 Method **17**
4.1 Camera and settings 17
4.2 Face detection and traction 19
4.3 Region of interest 19
4.4 Spectrum estimation 20
4.4.1 Sampling methods 20
4.4.2 Normalization 21
4.4.3 Zero-padding 21
4.5 Robust Estimation of Heart Rate 22
4.6 Implementation Aspects 23
4.7 Evaluation 24
4.7.1 Reference ECG 24
4.7.2 Statistical Analysis 24
4.7.3 Computational Time 24

5 Results **26**
5.1 Output of the Program 26
5.2 Camera 28
5.3 Lighting conditions 28
5.4 ROI methods 28
5.5 Signal processing 31
5.5.1 Window methods 31

5.5.2 Sampling methods 31
5.5.3 Zero-padding 32
5.5.4 Resolution of frequency spectrum 34
5.6 Estimated Heart Rate 34
5.7 Segmentation parameters 36
5.8 Performance of the developed program 36
5.8.1 Tracking changes in HR 36
5.8.2 Statistical Analysis 40
5.8.3 Outlier rejection 41
5.9 Graphical user interface 42

6 Discussion **43**
6.1 Ethics 47

7 Conclusions **49**

8 References **50**

9 Appendix **53**

1 Introduction

Measurements of blood volume pulses in microvascular tissues can be achieved using an optical technique called photoplethysmography (PPG). From the PPG signal heart rate (HR) can be extracted. In the past two decades the possibility of measuring PPG without body contact has been developed using cameras. This method is known as remote PPG (rPPG), video PPG (vPPG) or imaging PPG (IPPG), in this report it is referred to as IPPG.
When using IPPG, measurements of HR can be easier accessed since the needed devices are more widely-spread than the traditional contact measurements, such as conventional PPG or electrocardiography (ECG). According to Sun and Takor [1], contact forces from for example fingerprobes or handheld probes used in conventional PPG have been found to deform the arterial wall and thus impacted the results of measurements with contact methods. Contact measurements might also cause nervousness or uncomfortableness which would also impact the results. These problems are avoided or reduced when using measurements that do not require contact with the patient. Other advantages of non-contact measurements of HR are that they can monitor several spots at the patients in the same time without compromising the mobility of the patient, that the patient does not have to be aware of when the monitoring starts in situations like police interrogation and that evaluation of skin healing processes may be performed.
This report aims to present a method of developing an IPPG system with investigations into the state of the art of this area. Different algorithms that may be used are presented, and the basic requirements of the system, including requirements of the camera and illumination source, have been presented. Many of the studies today are based on off line video recordings. With this study, we aim to accomplish a system that can be used for real time monitoring of heart rate. The aim is to develop a robust system that is not easily disrupted by noise of different kinds. One camera is to be used, thus the presented method is not expected to present results if the patient would leave the field of view of the camera or turn the face away from the camera. The system is intended to be able to work as a demo for displaying the IPPG technique. For this reason, the system should be constructed to be as simple and ready-to-use as possible, without having to change much in order to adapt it to different conditions.

2 Background

2.1 Heartbeat

Heart rate (HR) is the number of heart beats within a certain time interval, usually one minute. The pulse refers to the number of expansions and contractions of the arteries within one minute, and is thus a measurement of the heart rate. Heart rate variability (HRV) is the variation in the time intervals between two following heart beats, [2]. HRV is typically measured between the R-peaks of an ECG signal and reflects conditions of the patients automatic nervous system [3]. HRV is often used to give information about cardiac conditions as well as a patient's mental stress [4].

According to Tominaga, [5], the light reflected from the skin consists of light directly reflected by the epidermal layer as well as diffuse backscattered light. The directly reflected light is independent of the pulsations, but the backscattered light contains information from the dermal and subcutaneous layers, including pulsatile information.

2.2 PPG

Since IPPG is based on the technology of PPG, some background information on PPG will here be given in order to better understand the development of IPPG. PPG was first proposed in 1938 by Hertzman [6]. PPG is a non-invasive technique used to measure changes of blood volume during the cardiac cycle. PPG basically consists of a light source and a photo detector. The light source illuminates the studied tissue, most commonly using a light emitting diode (LED). Usually wavelenghts in the red or near infraread spectrum are used (around 800-1000 nm) since this causes a minimal absorption of the light in blood, but recent studies have showed that green light can enhance the pulsatile information and reduce movement artifacts [7].
The photo detector is sensitive for changes in intensity of the detected light. If the photo detector is placed on the opposite side of the tissue compared to the source it detects the variations in intensity of the transmitted light, and the PPG can thus be called to be in transmission mode. If the photo detector is placed right next to the source it is said to be in reflection mode, and thus detects intensity variations of the reflected light, see Fig. 1. Different tissue components are differently sensitive to different optical wavelengths, and this property is taken advantage of in PPG. The content of a PPG signal can be divided into two subparts: the very slowly varying baseline ("DC") caused by for example respiration and venous flow, and the pulsatile waveform ("AC") which is caused by changes in the blood volume with each heartbeat, see Fig. 2. According to Sun and Takor [1], the AC-component of the signal only measures about 1 percent of the total intensity of the signal.

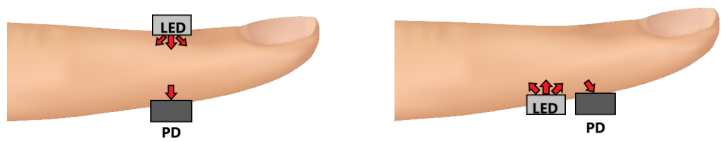

Figure 1: Transmission and reflection mode of a PPG measurement of a finger, proceeded from figure in [8].

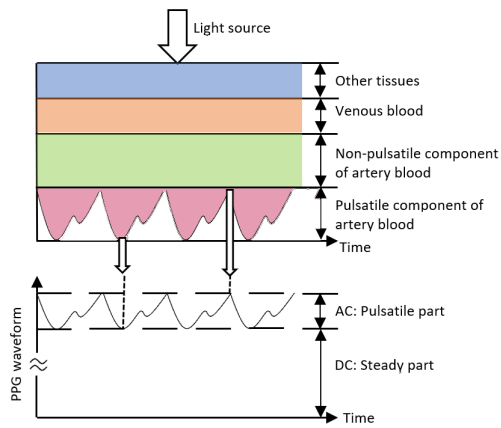

Figure 2: AC and DC components in the PPG signal, proceeded from figure in [1].

During a cardiac cycle the heart pumps blood to the lungs and body, and this results in a raise of blood volume in the capillaries of the skin surface. When a light is emitted to the skin it will be more attenuated as a result of the larger blood volume in the capillaries, and it will then be less attenuated when the blood returns to the heart [1]. This pulsing motion will be seen as the AC component of the PPG waveform.

3 Theory

In similar ways as in conventional PPG systems, a camera can detect reflected light variations that origin from changes in blood volume in micro vascular tissue. This non-invasive optical technique for detecting PPG signals has been proved to work efficiently for measurements of pulse rate [9], respiration rate [10], pulse rate variability [10] and blood oxygenation [11].

There are other non-contact techniques of HRV measurements, such as laser doppler and microwave doppler, but compared to them IPPG is a cheaper method that does not require as advanced equipment.

3.1 Camera

The cameras used in IPPG-systems can be divided into three types: cellphone cameras, simple digital cameras, and high definition (HD) cameras [1]. The systems using cameras inducted in cellphones commonly uses the flash light, composed of white light emitting diode (LED), as light source. The user is then supposed to cover both the LED and camera with his/her finger in order for the system to obtain measurements of HR. According to a study composed by Jonathan and Leathy [12] these systems works well for HR-assessment, and they have been developed to several commercial products, amongst which for example "What's my Heart Rate" and "Cardio Buddy".

The remaining two systems uses non-contact measurements methods, and are thus more relevant for the matter of this report. The simple digital cameras are based on a consumer close level which also includes webcams. The illumination source of these systems is simply ambient light. The advantages of these systems are that they are cheaper and easier to access than more advanced camera systems, but to the best of our knowledge it has not been performed enough studies to make sure that variations of ambient light does not effect the system in any way. Sun et al [13] could draw the conclusion that variations in the intensity of the ambient light had no interference with either systems capacity of obtaining accurate measurements, but in order to verify the result more studies on the subject would have to be done. Verkruysse et al. [14] showed that video recordings of the face taken with a simple digital camera using ambient light contains informative PPG signals. They may be used for different purposes in medical care, for example remote measurement of vital signs such as HR and respiration rate (RR), and for characterization of vascular skin lesions. The study also showed that the green channel contains the strongest plethysmographic signal, which can be explained by the fact that (oxy-) hemoglobin absorbs green light better and penetrates the skin to a sufficient level for reaching the vasculature. It was thus stated that the red and blue channels can contain complementary information.

The HD-camera-based systems were used in the early development of IPPG and

traditionally used red light and near infrared (IR) light [1]. Many of these systems work only in still condition and the reduction of motion is thus not ideal. Today the HD cameras have a high sampling rate and compared to more simple cameras have higher sensitivity and have better capacity of collecting several physiological parameters such as blood oxygen saturation [13].
Sun et. al. [13] performed a comparison between a high sensitivity complementary metal oxide semiconductor (CMOS) camera and a cheap and simple web cam using ambient light in both cases. Interestingly enough the study showed no significant difference in the ability to obtain HR in patients having undergone different amount of exercise. As mentioned above, the more advanced CMOS camera traditionally uses a customary light source and have then given results with better sensitivity than a web cam typically has.
Another matter to take into consideration is how many frequency bands that should be used. The most commonly used camera contains three channels; red, green and blue (RGB). A study performed by McDuff et. al. [15] showed advantages of using a five channel camera, more about this in section 3.5.
As previously mentioned, the AC component only stands for a small part of the total intensity of the signal. Therefor it is of great importance that the camera has a high sensitivity over the spectral range of the used illumination source. Since different frequencies and exposure times may be of value to different applications, the user must also be able to vary those parameters.

3.2 Lighting conditions

Fletcher et. al. [16] has published an article comparing different types of lighting (natural sunlight, compact fluorescent, and halogen incandescent) and varying brightness using two different smart phone cameras. Results showed that the optimum lighting types of the three compared ones were compact fluorescent and natural sunlight, with no statistically significant difference between the two. The optimum brightness was within 1000 lux to 4000 lux, and the reason for growing numbers of error above 4000 lux might be color saturation.

3.3 Detection and traction of region of interest

In order to be able to find and follow a face in straight vertical and horizontal movements (no turning of the head) the first step is to identify the face and choose a certain region of interest (ROI). There are many different methods for this, and they can be divided into manual or automatic detection. A manual selection takes time and is usually not able to track a moving face [1]. One commonly used method for automatic face detection has been presented by Viola and Jones [17]. The Viola and Jones (VJ) algorithm is based on a principle of so called Haar-like features, see Fig. 3. The intensity is compared between different regions in the face, and by

different premises such as that the eye region is darker than the cheeks and nose, the features of the face can be localized. For a two-rectangle feature, containing one white side and one black side of the same size, the value of the feature is calculated as the sum of the pixels at the white part subtracted from the sum of the pixels at the black part of the rectangle. An example of a two-sided feature can be seen as the middle part of Fig. 3. A three-rectangle feature, as can be seen in the right-most part of Fig. 3, contains of the rectangles of the same size. The feature is then calculated as the sum of the two outlying rectangles subtracted from the center rectangle.
The rectangle features are computed using an intermediate representation of the image called *Integral Image*. Together with a combination of complex classifiers in a cascade that sorts out background regions and focus the work on more interesting areas, the VJ algorithm proved to be comparably accurate and much faster than the previous face detection systems. The VJ algorithm is mainly developed using frontal face position, which might cause problems when the face turns away from the camera.

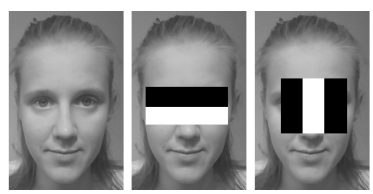

Figure 3: The first feature (marking the difference in intensity between the eyes and cheeks) and second feature (marking the difference in intensity between the eye region and the bridge of the nose), inspired by [17].

Feng et al. proposed another automatic detection method [18], where ROI selection on the subject's cheeks, using the VJ face detector, was combined with a speeded-up robust features point tracking. Their method obtained significantly higher accuracy in the PPG signal compared to other existing methods.
If the face would be treated as a rigid body with no restrictions of motion, it would have six degrees of freedom (DOF). The motions could then be divided into six types, as shown in Fig. 4: yawing, pitching, rolling, heaving, swaying and surging. According to [18] noise that originates from different types of face movements (yawing, pitching, rolling and surging) can be removed when a good ROI tracking mechanism is applied. One method that compensates for some of these types of movements, yawing and rolling, is the Dlib-ml face detection [19]. Dlib-ml face detector is also able to detect faces with glasses and bangs. Wu et al. [20] used the Dlib-ml face detector and combined it with acquirements of the center points of the eyes and mouth as well as a rotation of the detected facial rectangle that

followed the straight line between the center of the eyes in order to compensate for rolling of the head. The method also contained other algorithms such as template matching method. Wu et al. finally achieved a robust face detection and traction that was resistant to all types of head movements.

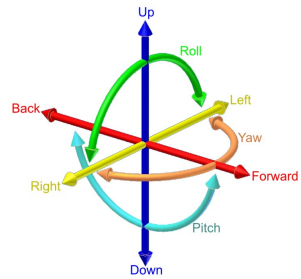

Figure 4: 6 DOF, where swaying is represented by movement along the right-left axis, heaving by movement along up-down axis and surging by movement along forward-back axis.

Once the face has been correctly detected there are different methods to follow and track the localization of the face. One of the most common algorithms for continuous tracking is the Kanade-Lucas-Tomasi (KLT) algorithm [21]. KLT algoritms calculates the displacement of detected features from the first frame to the proceeding frames.

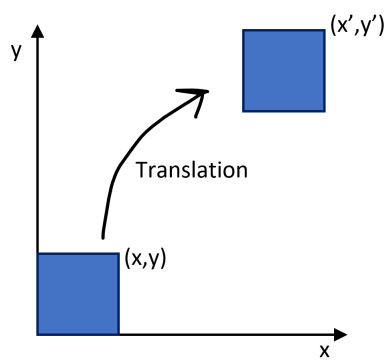

Figure 5: Translation movement of frames, with inspiration from [21]

If one corner point in Fig. 5 holds the coordinates (x,y) in the first frame, and is displaced by a variable vector $[a_1, a_2]$, the corresponding corner point in the next frame is the sum of the initial point and the displaced vector. The coordinates of the displaced corner point (x',y') will then be as presented in (1).

$$x' = x + a_1$$
$$y' = y + a_2 \tag{1}$$

A warp function is then used to calculate the displacement with respect to each coordinate. The warp function contains coordinates and a displacement parameter p, and is denoted as $W(x;p) = (x + a_1; x + a_2)$. Using the coordinates of feature points in the first frame as a reference, the next tracking points in proceeding frames are found by taking the difference between displacement and the previous point.

3.4 Spatial averaging

Wang et al. proposed two alternative methods to use the spatially pruned IPPG sensors [22]. The first alternative is to average the inliers. This method is often called *spatial averaging* and is the most common method despite the fact that it compromises the spatial resolution [1]. It was first introduced by Verkruysse et al. [14] and has proven to significantly improve the signal-to-noise ratio (SNR) when there are small motion artifacts involved [1].

$$I(n) = \frac{\sum_{x,y \epsilon \Omega} I_{x,y}(n)}{N_\Omega} \tag{2}$$

Equation (2) shows calculations of the spatial average of all pixels belonging to the subset Ω, where $I_{x,y}(n)$ is the intensity of the n:th pixel, and N_Ω is the number of pixels in the subset, defined by the ROI.

The second method proposed by Wang et al. is *Spatial concatenation* [22]. This method intends to first extract independent pulse signal from the pixels within the ROI. The pulse signals are then to be ranked after their distance to the mean and those that have similar ranking are concatenated. The signal-traces at the top should then be the most reliable ones. Finally after additional post processing the multiple pulse traces are combined to one robust pulse signal.

3.5 Color channel selection

Poh et al. [9] used a red, green, blue (RGB) camera from a short distance to estimate HRV features. They found that the resulting signal was limited by frequency band resolution. McDuff et al. [15] proposed a method using a 5 channel camera that included cyan (C) and orange (O) with the RGB bands. The RGBCO turned out to have better accuracy compared to an RGB camera, and more specifically the most accurate combination was with the GCO channels. The green channel contains less noise and has a stronger pulse amplitude than red and blue, but as previously mentioned some complementary information might be lost if only

investigating the green channel.
The different channels can be combined by varying methods. Poh et al. proposed using independent component analysis (ICA) in order to linearly transforms the channels to components that are maximally independent of each other [10]. The resulting components of this method would then represent different artifacts as well as the pulse signal, separately.
Lewandowska et al. proposed a different solution using principal component analysis (PCA) for defining three independent linear combinations of the three color channels channels [23]. They could draw the conclusion that PCA was less computationally complex and took less time for calculations compared to ICA. For pulse rate measurements PCA showed similar accuracy as ICA. The conclusion was therefor drawn that PCA might be an appropriate method for real-time applications.
Alghoul et al. compared two new methods for HRV extraction, whereas one was based on ICA and the other on Eulerian Video Magnification (EVM) [2]. They were pioneers in using EVM technique for extraction of physiological parameters from PPG signals, and they tested it on 12 subjects with varying skin color and ethnicities. Their findings showed that the EVM technique had very good result in time domain parameters, but high frequency noise could not be eliminated. The ICA based method did not have the same problem with high frequency noise, since the noise was separated from the pulse signal into independent components. The EVM technique used spatial pooling which combines adjacent pixels, and the high frequency noise could not be separated from the PPG signal. The conclusion was drawn that their proposed ICA method was most convenient and gave the most clean PPG signal with good results in both time and frequency domain.
With blind source separation (BSS) techniques such as ICA and PCA it would however take additional investigations to identify the component containing the pulse signal. Usually, it is assumed that the signal showing strongest periodicity is the pulse signal [24]. However, this assumption will be problematic during periodic motion, such as in fitness setting. It also requires a longer observation interval in order to have good enough resolution in frequency domain, which makes adaption to quickly altering statistics impossible [24]. The BSS techniques can only present as many independent components as there are observations [1]. This means that using a RGB camera would result in three different components but with a five color channel camera, two additional components can be extracted. This would allow for more different sources of artifacts to be extracted, thus a higher probability of resulting in a more pure pulse signal.
In 2013 de Haan et al. proposed an alternative method to avoid the risky component selection heuristic that might fail with periodic motion [24]. It is based om eliminating the specular reflection component by using color difference (chrominance) signals under the assumption of standardized skin-tone. The chrominance-based

IPPG method considers the pulse as a linear combination of three color channels. This method has proved to be superior to the BSS methods in adapting to changing conditions and performing with short latency as well as it shows the highest accuracy.

3.6 Filtering

In order to eliminate as much noise as possible, different types of filters can be applied to the IPPG signal. A normal pulse rate for a healthy person is within 40-240 beats per minute (bpm). Frequencies outside of this range can be removed. One example of a filter that have been successfully applied to reduce noise in IPPG signal is a simple band-pass filter. Verkruysse et al. [14] presented a method that used a band-pass filter with 4th order Butterworth coefficients in a phase neutral filter, and it resulted in robust and clear PPG signals. Wang et al. took advantage of the fact that in each moment the instant pulse frequency should be concentrated to a yet smaller range, such as 70-80 bpm [22]. Therefor an adaptive band-pass filter was applied by using real-time pulse rate information which could limit the band-pass filter range even further. Other filters that have shown good results in the field of IPPG noise reduction are average filters, used for example by [10], Kalman filter, as used by [20], and wavelet denoising, as presented in [25].

3.7 Extraction of pulse signal

According to Sun et al., the extraction of physiological signals from the processed PPG signal can be divided into two methods; heuristic and learning based methods [1]. One heuristic method that is commonly used is transferring the signal to frequency domain, and simply detecting the highest peak withing the range 40-240 bpm. In order to be able to get more information about the temporal localization of a signal's spectral components a joint time-frequency analysis can be used. Hulsbusch and Blazek, [26], performed a study where they reverted to joint time-frequency analysis by using a Wavelet Transform. This transfers the time signal into 3D time-frequency space which makes it possible to study different characteristics of the signal.
Another heuristic to extract pulse signal is by detecting local maximum in a moving window. This has been done by among others McDuff et al. [15]. One negative aspect of this is the fact that it is more sensitive to motion induced noise.
Hsu et al. [27] proposed a novel learning based method for pulse rate detection. They argue that by choosing only the frequency with highest amplitude in the frequency domain, valuable information about heart beats and noise might be lost. Instead they propose support vector regression over the prior low and mid-level features as well as multiple feature fusion strategies. Comparing with heuristic methods the detection error was significantly reduced using this method.

3.8 Welch's method of spectral estimation

For a signal with finite samples, the power spectrum can not be optimally estimated as the spectrum of the true signal. Using the periodogram as power spectrum is connected with a variance that is proportional to the square of the value of the spectrum. This means that with an increasing number of N data points the variance does not decrease. A method suggested by *Welch*, proposes splitting the data into smaller segments of length L, with the starting points of these segments D points apart, [28]. For reference see Fig. 6. If K number of segments are covering for the whole signal, then $N = L + D(K-1)$. The overlap degree is defined as $OF = \frac{D}{L}$.

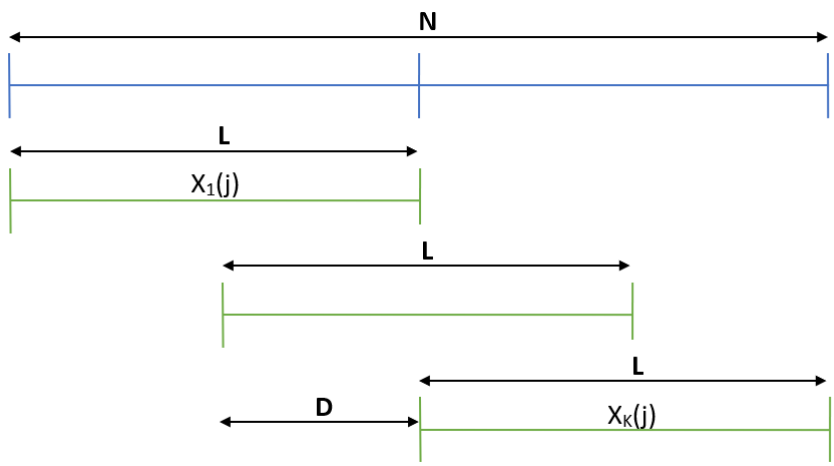

Figure 6: Illustration of segmentation in Welch's method, inspired by [28].

Assuming a signal $X(j), j = 0, ..., N-1$, that is a sample from a stationary, stochastic, second-order sequence. Dividing $X(j)$ into sequences, starting with $X_1(j), j = 0, ..., L-1$, then implies

$$X_1(j) = X(j) \quad for \quad j = 0, ..., L-1, \tag{3}$$

and

$$X_2(j) = X(j+D) \quad for \quad j = 0, ..., L-1. \tag{4}$$

In the same way,

$$X_K(j) = X(j + D(K-1)) \quad for \quad j = 0, ..., L-1. \tag{5}$$

For each segment a modified periodogram is calculated applying a selected data window. This step often implies a loss of information since the windowing functions in many cases takes more influence of the data in the center pieces of the set than of the outer parts. This effect is however reduced by the overlaps since the windowing effect is spread out over several segments. A discrete Fourier transform is applied and the squared magnitude of the results are then calculated, thus obtaining the periodogram of every segment. Finally, each periodogram is averaged in order to reduce the variance of the individual power measurements.

3.9 Resolution of frequency spectrum

The resolution of the frequency spectrum obtained using FFT can be divided into two separate parts. The first aspect is the minimum distance between two frequencies that can be resolved. Referring to this aspect as frequency resolution. R_f, it can be defined by 6.

$$\Delta R_f = \frac{1}{T}, \tag{6}$$

where T is the time length of the data signal. The second aspect of resolution of the frequency spectrum is hereon referred to as spectral resolution, R. This is defined as the number of points in the spectrum, as can be seen in 7.

$$\Delta R = \frac{f_s}{N_{fft}}, \tag{7}$$

where f_s is the sampling frequency and N_{fft} the number of FFT points.
Welch's method yields estimates that are spatially placed 1/L units apart. In order to improve the spectral resolution zeros may be added to the windowed sequences before taking the Fourier transform [28]. This method is called zero-padding. Adding L' zeros to the end yields sequences of length $M = L + L'$. The estimates will then be spatially placed at 1/M units apart instead. Note that zero-padding only affects the spectral resolution. The frequency resolution is not improved.
When time-domain data is zero-padded with a fitting amount of zeroes, the waveform gets a power-of-two number of samples. For a waveform with a power-of-two length, radix-2 FFT algorithms may be used. This type of algorithm are very efficient and significantly decreases the processing time.

3.10 Statistical analysis

According to Blom et al., [29] one statistical model which is applicable to this setup is samples in pair. It can be used to determine the mean difference between two sets of observations using different methods.
The setup for this model can be seen in Table 1. (8) shows the mean value of the

difference between the reference and estimated pulse. It can be seen as the mean value of a set of observations from a larger data set which is normal distributed with the distribution parameters as displayed in (9). The standard deviation for this model can be estimated using (10). The deviation of the larger dataset is unknown. For this reason, Student's T distribution function may be used to estimate the deviations in a conservative way. The model for calculation the confidence interval is described in (11). [29]

Object i	**1**	**2**	**. . .**	**n**	**obs. of**
x_i	x_1	x_2	...	x_n	$X_i \in N(\mu_i, \sigma_x)$
y_i	y_1	y_2	...	y_n	$Y_i \in N(\mu_i + \Delta, \sigma_y)$
z_i=y_i-x_i	z_1	z_2	...	z_n	$Z_i \in N(\Delta, \sigma)$

Table 1: Statistical model of samples in pair

$$\Delta^* = \overline{z}, \tag{8}$$

where Δ^* is the approximation of the mean difference between the two methods.

$$\Delta^* \in N(\Delta, \frac{\sigma}{\sqrt{n}}), \tag{9}$$

where σ represents the standard deviation and n is the number of samples.

$$\sigma^* = \sqrt{\frac{1}{n-1}\sum_{i=1}^{n}(z_i - \overline{z})^2} \tag{10}$$

$$I_\delta = \Delta^* \pm t_{\frac{\alpha}{2}}(n-1)\frac{\sigma^*}{\sqrt{n}}, \tag{11}$$

where $t_{\frac{\alpha}{2}}$ denotes the two sided t-distribution for the significance α.

4 Method

Below follows a review of the process of the designed program. All tests of the program were performed using simultaneous recordings of 3 lead ECG. The computed pulse rates of our program were then compared to the heart rate measured by ECG.
In Fig. 7 and Fig. 8 an overview of the steps in the developed program can be seen.

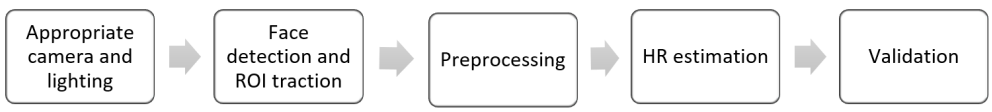

Figure 7: Overview of the process

4.1 Camera and settings

In this project, an HD camera from Logitech has been used, model C920 HD Pro Webcam. *MatLab Support Package for USB Webcams* has been used in order to get the video transferred to MatLab [30]. Since the aim of this project is to construct a simple and easy-to-use system this camera was found to be satisfying our needs. For the same reason, a simple system with as few components as possible was desired. Therefore, the system has not been limited to any specific lighting conditions, but works adaptive to the surrounding light.
All tests presented were conducted at resolution 640x480 pixels and at an uncapped frame rate. The camera thus goes under the definition of simple digital cameras, as described in section 3.1. If a camera with higher possible frequency were to be used the vectors would contain more values.
The used camera holds automatic functions for optimizing white balance and focal length. However, if these functions were to be used during the collection of data in our program, there is a big risk that the varying camera settings would interfere with the program. On that account, the camera modes for auto-focus and automatic white balance were used during the first sample. The optimized values for focal length and white balance were then preserved throughout the rest of the program since the light was assumed to be invariant during the time of the recordings.

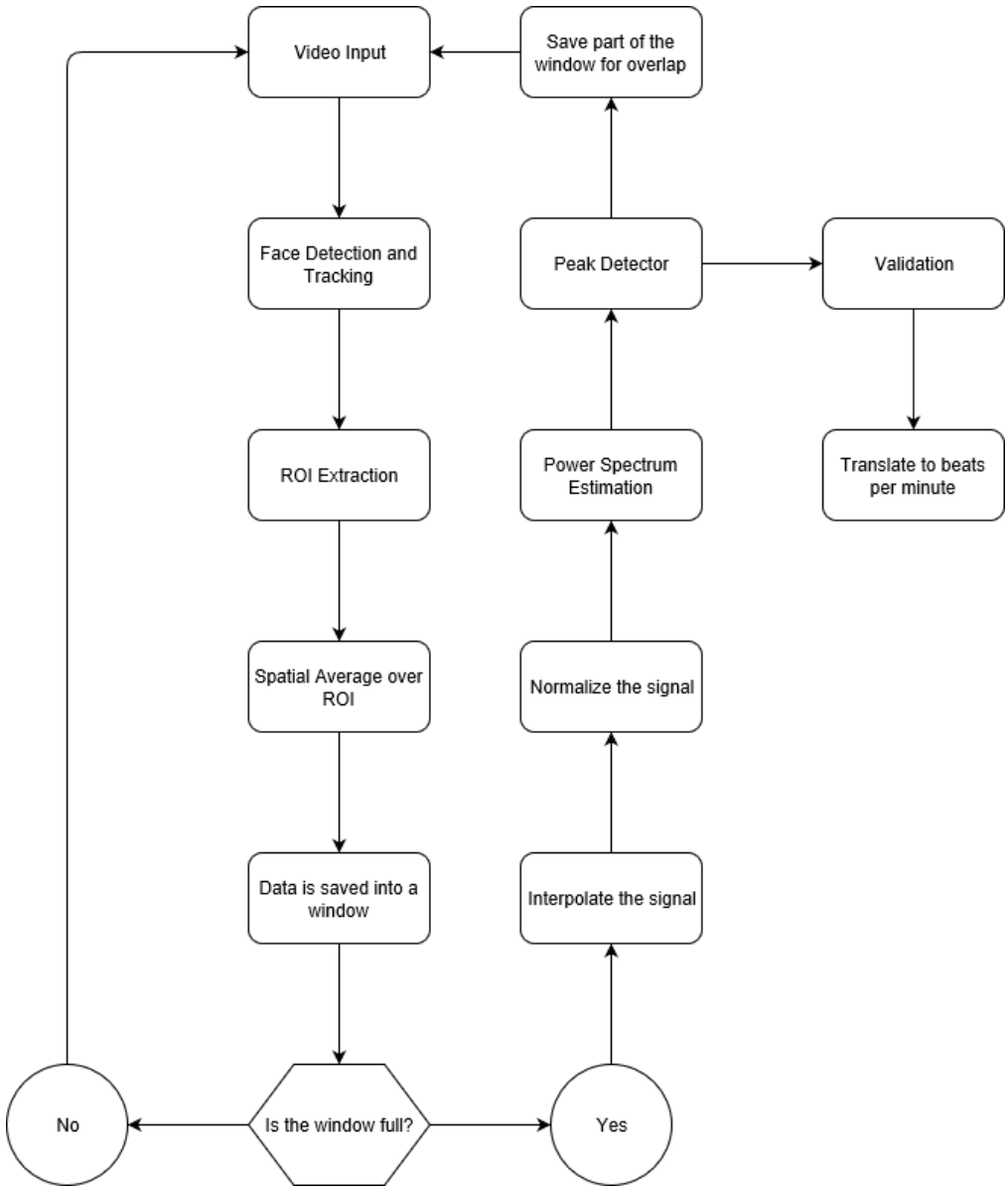

Figure 8: Flow of data in the process

4.2 Face detection and traction

A commonly used method for automatic face detection as presented by Viola and Jones, [17], and described in section 3.3, has been applied to the frames collected from the webcam. The reason that this algorithm was chosen is that it was easy to understand and apply to our project and works good enough for the intentions. When a possible face has been found - the program is paused and a picture is shown to the user asking if the correct face is displayed within the frame. If not, the face detection is restarted and the user gets the same prompt once more. Once the correct face has been detected, the KLT algorithm, as described in section 3.3, has been used to track the face between the frames. This has been done to ensure that the acquired signal contains the same region regardless of any movement.

4.3 Region of interest

According to a study performed by Taylor and Palmer, [31], the areas with highest density of blood vessels are the finger tips, followed by the face (especially the cheeks and forehead). Since the face is usually an uncovered part of the body it is also easily available for remote video recordings. Since the regions of the eyes, possible facial hair etcetera can be expected to not show alternations in similar frequency range as the skin color variations, a measurement of 60 percentage of the width of the face and the full height has been proposed. This method is later to be referred to as *ROI method 1* and is mathematically expressed in (12) and (13). It can be seen in Fig. 9. A similar method has been used by McDuff et al. in 2017 [32]. Our proposed method has been compared to a setup measuring only on the forehead, referred to as *ROI method 2*, see (14) and (15). This ROI is displayed in Fig. 10.

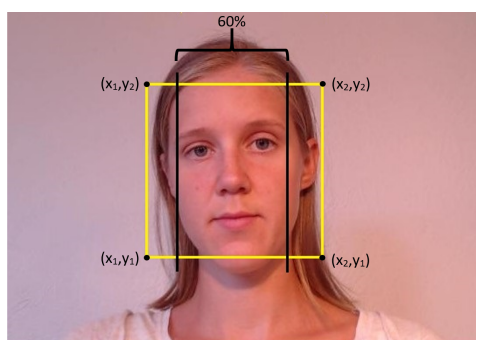

Figure 9: ROI method 1

$$x \in [x_1 + (x_2 - x_1) * 0.2, x_1 + (x_2 - x_1) * 0.8] \tag{12}$$

$$y \in [y_2, y_1] \tag{13}$$

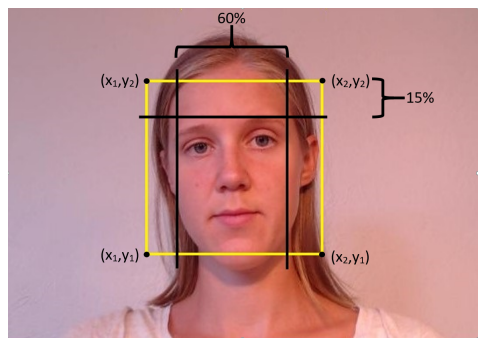

Figure 10: ROI method 2

$$x \in [x_1 + (x_2 - x_1) * 0.2, x_1 + (x_2 - x_1) * 0.8] \tag{14}$$

$$y \in [y_2, y_2 + (y_1 - y_2) * 0.15] \tag{15}$$

4.4 Spectrum estimation

The green color channel has been extracted for further analysis. The pixels within the chosen ROI of green color have been spatially averaged, as described in section 3.4, and the resulting value has then been saved in a vector.

4.4.1 Sampling methods

In order to obtain as evenly sampled frames as possible two different methods have been proposed. The first method, further on referred to as *Sampling Method 1*, is based on having an certain equal time stamp between each taken image from the live video sequence. An image is supposed to be processed every 0.05:th second, and until this the system is on hold.
The second method, to be referred to as *Sampling Method 2*, uses interpolation in order to avoid the problems that might occur in later stages if unevenly sampled frames are processed. Linear interpolation is simple and does not introduce any adaptations into the system, and therefor this method has been used

in the program. To determine the appropriate numbers of interpolation points both double and four times the number of sampled points has been tested. The goal was to get a good spectral resolution without using too much processing power.

4.4.2 Normalization

In order to remove the DC-component, the elements of the vector were normalized, as can be seen in 16.

$$\tilde{I}(n) = \frac{I(n) - \bar{I}}{\sigma_I}, n = 0, 1, ..., N_k. \tag{16}$$

where, $I(n)$ is the intensity of the n:th sample and the value of N_k varies depending on the number of samples during the period. σ_I denotes the standard deviation of the set, as presented in section 3.10.

4.4.3 Zero-padding

Zero-padding as described in section 3.9, has been applied to the signal with varying numbers of zeros added. In order to send in a power of two number of samples, different methods were tried. *Zero-padding method 1* involved sending data by adding zeros up to the closest radix, 2^x. *Zero-padding method 2* involved adding zeros to the second next radix, 2^{x+1}, which would result in at least 50 percent of the vector containing zeros. Using *Zero-padding method 1* the data set will be padded with fewer number of zeros.
The data was then segmented into M segments of equal size, $\tilde{I}_M$(n), for varying numbers of n, see 17. For each of these segments the power spectrum, $S_{x,M}(f)$ was calculated using a DFT algorithm. After this the mean of the results for each frequency was calculated and the result was saved, according to Welch's method for calculating the power spectrum of a signal as described in section 3.8. Note that $X(j)$ in equation (3)-(5) is in this case the intensity $S_x(f)$, where $f = 0, ..., L-1$. Different amounts of overlap have been tested in order to determine the optimal value.

$$S_{x,M}(n), n = 1, 2, ...N_k/M, \quad for \quad 1 \leq M \leq 4, \tag{17}$$

where N_k is the total number of samples during the period.

4.5 Robust Estimation of Heart Rate

The peaks of the power spectrum within the interval 0.67-3 Hz (40-180 bpm) were detected, of which the highest peak was initially assumed to hold the heart rate information. The detected peak, $f(n)$, in Hz was translated to $h(n)$ in bpm.

In order to as much as possible avoid faults which might occur in different parts of the system, a few different safeguard methods have been implemented. If there would be an unexpected delay in the acquirement of the signal, problems with the interpolation would occur since many values in one section would be estimated from a small set of data points. This would cause large problems further on in the system. Therefore if the system detects a longer delay than 0.2 seconds, the collected data up to that point is transferred to the signal processing part and the window is emptied and reset.
First of all, the system needs to verify that the detected peak really is a single peak and not the first high value on the downward side of a top outside of the chosen interval. In order to avoid this problem, the intensities of points on either sides of the assumed peak must be lower than that of the assumed peak, as described in equation (18). If this is not true, the second highest peak within the interval will be investigated. This phenomenon can be observed in some of the spectrums in figure 17b. Compare the peaks at around 1-2 Hz to the height of the leftmost part of the spectrum.

$$S_x(h(n-1)) < S_x(h(n)) < S_x(h(n+1)) \tag{18}$$

If the acquired heart rate, $h(n)$, deviates more than 10 beats per minute from the previously calculated heart rate, stored in a variable $h_r(n)$, the second highest peak is instead tried in the same way, see 19.

$$h(n) \in [h_r(n) - 10, h_r(n) + 10] \tag{19}$$

The intensity of the selected peak, $S_x(h(n))$ is compared to the total intensity of the system, $S_{x,tot}(h(n))$. If the chosen peak contains less than 20 percent of the total intensity the peak is considered not to be reliable and undergoes further testings to determine if it is distinct enough. The intensity of the chosen peak is then compared to the intensity of the second highest peak within the interval, $S_x(h_2(n))$. If the intensity of the chosen peak neither exceeds 10 percent of the total intensity nor 120 percent of the intensity of the second highest peak, no value is presented during this iteration, see (20).

$$h(n) = \begin{cases} \begin{cases} h(n) & \text{if} S_x(h(n)) \geq 0.10 * S_{x,tot} \\ \begin{cases} h(n), & \text{if } S_x(h(n)) \geq 1.20 * S_x(h_2(n)), \\ none, & \text{if } S_x(h(n)) < 1.20 * S_x(h_2(n)) \end{cases} & \text{otherwise} \end{cases} \end{cases} \tag{20}$$

4.6 Implementation Aspects

Two different methods for the number of collected samples to fill the vector with have been used and compared, *Window method 1* and *Window method 2*. *Window method 1* proposes collecting a fix number of samples before continuing to following processing. The process of adding spatial averages to a vector continues until the vector is filled with 800 values (thus corresponding to 800 pictures). *Window method 2* does not fill the vector with a fix number of samples, but have a varying size. Instead, the recorded time is fixed to 30 seconds. With a frame rate of 30 Hz the width of the window thus varies around 900 samples.

After the data processing, the values in the last part of the window were saved and were used as the first part in the next sequence, as can be seen in Fig. 11. The program runs L iterations until the user chooses to stop the program. Assuming a signal $X(l)$ for iteration l, $l = 1, 2, ...L$ that has been split into N segments, according to $X(l) = \sum X_1(l) + X_2(l) + ... + X_N(l)$. The segments will then be replaced by the following segment as defined in (21).

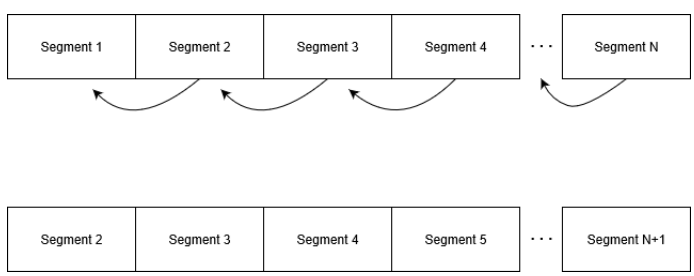

Figure 11: Segmentation in termination step and beginning of next cycle, with N number of segments

$$\begin{aligned} X_1(l+1) &= X_2(l) \\ X_2(l+1) &= X_3(l) \\ X_N(l+1) &= X_{N+1}(l) \end{aligned} \tag{21}$$

According to the waveform frequency resolution, as mentioned in section 3.9, the longer saved data stream the better the resolution. Splitting the signal into a larger number of N sections and only changing the last part would thus both increase the waveform frequency resolution and yield a smaller time until a HR can be displayed. However, since this is a trade-off between resolution and processing time, different numbers of sequences have been tested to find an appropriate number.

4.7 Evaluation

The different methods and parameter values were tested in order to chose the most appropriate settings for the program. Two recordings each on 9 subjects of varying ethnicities, genders and ages were taken during approximately two minutes. The ages varied from 18-64 years, and there were 5 men and 4 women. The persons have hereon been named person A-I.

4.7.1 Reference ECG

At the same time as the video recordings measurements with 3-leads ECG were performed to use as reference. The ECG used for reference measurements of HR was eMotion FAROS 360 using a sampling rate of 1000 Hz. The data from the ECG was then imported into Matlab using an EDF reader [33]. In order to evaluate the recorded ECG signals Pan Tomkins method has been used [34].

4.7.2 Statistical Analysis

The statistical model used for analysis in this project is samples in pair, as described in section 3.10. Referring to Table 1, x_i then refers to the estimated pulse and y_i refers to the heart rate measured by the reference ECG. The reason that this method has been used is that the pulse might vary much between the different subjects, and at the same time the difference between estimated and reference pulse is small in comparison. There is an expected correlation in the expected value. The model allows for testing if the expected value differs significantly from the reference pulse value versus the pulse estimated by the program.

4.7.3 Computational Time

The performance of the final program was tested in two different ways. The total time it takes to execute the processing steps using Matlabs tic-toc feature and how long the computation time is in the processing steps using Matlabs CPU-time feature. These values will depend a lot on what kind of unit the program is run

on. However the differential of these values will give an estimate on how different parameters differs. CPU-time is supposed to take into account parallelism by assuming that the system is using the processing cores equally.
For this trial a HP spectre laptop with a Intel I7-7500U dual core CPU with 4 threads running at 2.7 GHz on an 64-bit architecture was used, [35]. This means that the value for CPU-time might be off because it assumes that the system is able to use both CPU cores at most of the time. The value for computational time should then be divided by two at every instance to give an accurate measurement.

5 Results

The following results are obtained when using the most appropriate methods and parameters for the developed program. In section 5.3 to 5.8 a comparison of the different used methods and parameters is presented. In Table 2 an overview of the test parameters used in the different sections presented in this report can be seen.

5.1 Output of the Program

Tables with output values of pulses estimated by the program and the corresponding pulse measured by ECG can be found in Appendix, section 9. The difference between the reference pulse and the estimated pulse is presented in Table 3. Test E_2 has been left out since variations of light intensity during the recording interfered with the measurements. The light variations were due to a window drape that was moved aside by drafts. This also led to the subject turning his/her face towards the window and thus away from the camera. This was outside of the limits of this project and the results from this test has on this cause not been included in the statistical analysis of this report.

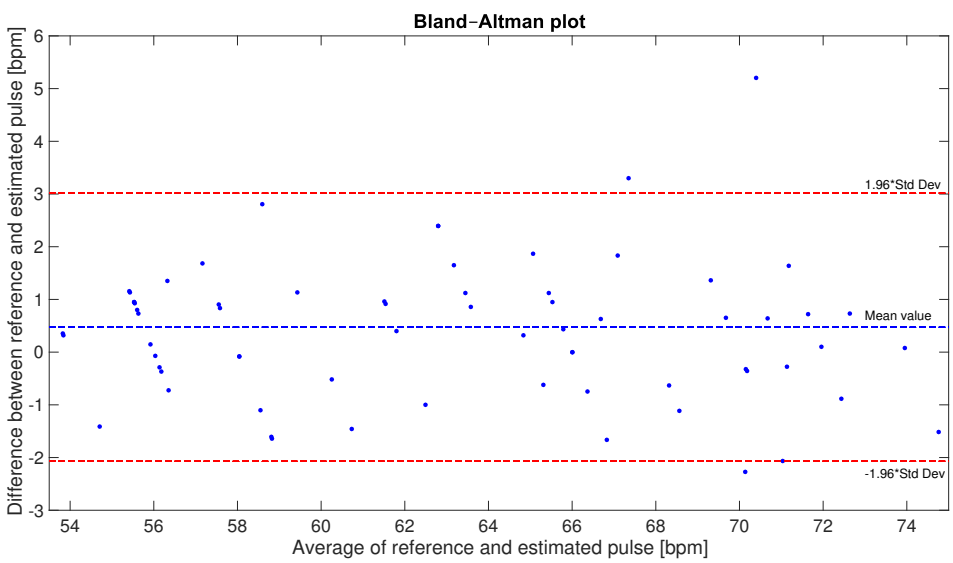

Figure 12: Bland-Altman plot

In Fig. 12 it can be observed that there is no significant dependency between deviation of estimated pulse from the reference pulse and average pulse. The difference between reference and estimated pulse seem to be randomly distributed

Test described in section	**ROI method**	**Window method**	**Sampling method**	**Zero-padding method**	**Welch's method**
5.3	2	2	2	2	Not used
5.4	Varied	2	2	1	2 sections, 50% overlap
5.5.1	2	Varied	2	1	Not used
5.5.2	2	2	Varied	Not used	Not used
5.5.3	2	2	2	Varied	Varied
5.5.4	Varied	2	2	Varied	Varied
5.6	2	2	2	2	Not used
5.8	2	2	2	2	Not used

Table 2: Overview of test parameters

Test number	ΔHR **0-30 s**	ΔHR **30-60 s**	ΔHR **60-90 s**	ΔHR **90 -120 s**	**Average of** ΔHR	**Mean absolute deviation**
A_1	0.73	5.20	3.30	0.10	2.33	2.33
A_2	0.63	-1.67	0.65	-0.32	-0.18	0.82
B_1	2.40	-1.46	-	1.13	0.69	1.66
B_2	2.40	0.40	-0.52	-1.64	0.16	1.24
C_1	1.36	0.92	0.95	0.95	1.04	1.04
C_2	-0.29	0.15	-0.72	-0.37	-0.31	0.38
D_1	-1.12	1.12	-0.62	0.32	-0.08	0.79
D_2	1.83	-0.75	1.86	0.85	0.96	1.32
E_1	0.64	-0.28	-0.36	2.28	0.57	0.89
E_2	23.48	1.60	-0.40	28.00	13.17	13.37
F_1	0.43	-0.06	0.00	0.43	0.20	0.23
F_2	1.12	1.92	0.96	1.65	1.41	1.41
G_1	0.83	1.68	-1.41	-0.08	0.26	1.00
G_2	0.80	0.73	1.16	1.13	0.98	0.96
H_1	-1.52	1.36	0.00	-0.64	-0.20	0.88
H_2	-0.88	0.08	1.64	0.72	0.39	0.83
I_1	-1.10	0.32	0.35	0.90	0.12	0.67
I_2	-0.07	2.80	-1.61	-0.08	0.26	1.14

Table 3: Statistics of deviations between reference and estimated HR for all performed tests, where $\Delta HR = HR_{ref} - HR_{est}$

over the averaged pulse. The dashed blue line is the calculated approximated mean value of the data set and the dashed red lines represent limits of which 95% of the averaged samples in the data set are expected to fall within.

5.2 Camera

Since it is of great importance that the time stamps are correct, a camera that gave access to this information had to be used. For this reason a C920 HD Pro Webcam from Logitech as described in section 4.1 has been used. The system was designed to work with any camera that has access to the time data along with the data stream. The test subjects were placed at a distance of about 1 meter from the camera lens.

5.3 Lighting conditions

Tests performed in different environments, and with different surrounding light sources, have shown the significance of good light from a good angle. Fig. 13a shows the conditions and environment of one test on subject A. As can be seen there are light sources above and right in front of the test person as well as daylight coming in from his right side. There is also daylight coming from behind the camera and behind the subject. This set up resulted in a very poor signal quality with a small SNR.

After the results of test on subject A, all subjects were placed in a room with a more limited number of light sources for their video recordings. Preferably with windows covered or after the sun set, to avoid interfering of daylight from windows. The locations of the continued tests can be seen in Fig. 13b and 13c. No further FFT spectrums with much noise that made the localization of the pulse peak difficult, were encountered.

5.4 ROI methods

A comparison between *ROI method 1* and *ROI method 2*, as presented in section 4.3, from test performed on test person B showed the results displayed in Fig. 14a and 14b. The methods were tested using a window with 6 segments with each a time limit of 5 seconds, using the method described in section 4.6. The tests were performed using Welch's method with 2 sections and a 50 percent overlap, and applying zero-padding with a power-of-two length. As can be seen, using *ROI method 2* gives a much more distinct peak as well as less noise throughout the spectrum. In Fig. 14a there are peaks at about 1.6-2.2 Hz that are not as noticeable in Fig. 14b. Comparing to the reference HR, these peaks can be concluded to arise from something other than heart beats. If the interference from these causes would have been slightly stronger, the output of the program could have resulted

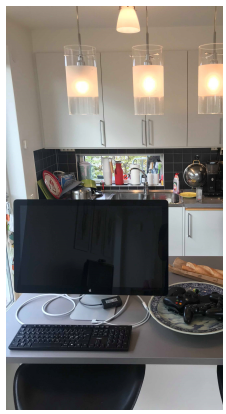

(a) Environment of one of the tests performed on person A, where A was placed on a chair behind the computer monitor

(b) Environment of test on subject D, E, G, H, I

(c) Environment of test on subject B, C and F

Figure 13: Environments used for recordings

in misleading HR estimation presented. It could also affect future estimations if the future true peaks would be ignored due to the validation parameters.
Since similar results were acquired from several different recordings of varying test persons and surroundings, *ROI method 2* was chosen as priority for the developed system. *ROI method 2* has been further tested on a person with much and covering makeup (test person H), as well as one person with glasses (test person I). The results of these tests can be observed in Table 3. As can be seen in Table 3, the difference between the estimated pulse and the ECG measured pulse are of similar range as for the remaining tests, and no problems were thus observed with either of these special cases. However, some difficulties were encountered when only measuring on the forehead, including measuring on people with bangs or big covering glasses. For this reason, usage of *ROI method 1* remained in the program

as an option for those cases when *ROI method 2* might be found challenging.

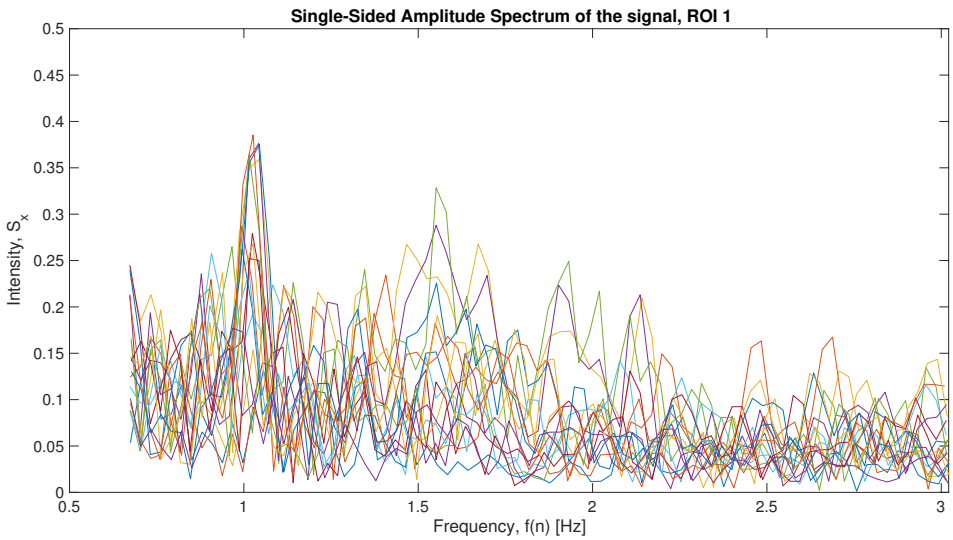

(a) *ROI method 1*

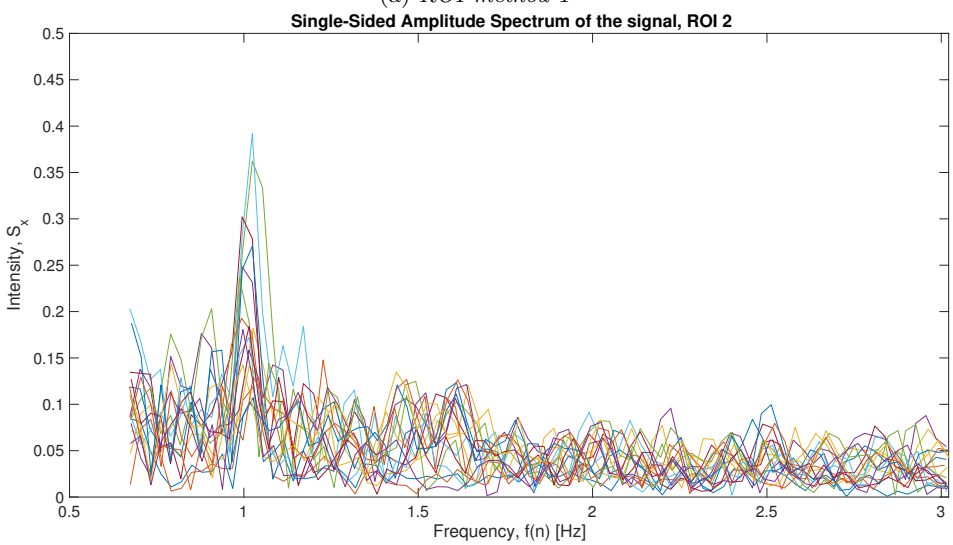

(b) *ROI method 2*

Figure 14: Spectrum from tests on test person B using *ROI method 1* and *ROI method 2*

Method used	**Length**	ΔR_f
Window method 1	75	0.067 Hz
Window method 1	150	0.033 Hz
Window method 1	225	0.023 Hz
Window method 1	300	0.017 Hz
Window method 2	2.5 s	0.066 Hz
Window method 2	5 s	0.033 Hz
Window method 2	7.5	0.022 Hz
Window method 2	10 s	0.017 Hz
Window method 2	12.5 s	0.014 Hz
Window method 2	15 s	0.011 Hz

Table 4: Comparison of frequency resolution, ΔR_f as presented in section 3.9, between *Window method 1* and *Window method 2*

5.5 Signal processing

5.5.1 Window methods

The results from using the different window methods is entirely dependent of the length of the samples and the number of sections used. If a too small window size is selected, a smaller data set will be examined at the latter stages of the program which will lead to lower spectral resolution. However a larger data set will force more data to be processed and potentially slow down the system.
No significant difference in estimation of HR has been noted when using *Window method 1* or *Window method 2*, as presented in section 4.6. On some computers where there may be a start up delay, *Window method 2* initially gives better results since it does not wait until it has enough samples. *Window method 2* was selected for the developed program.
The data in Table 4 has been collected using 6 Sections, without the use of Welch's method, from a set of recorded signals, sampled at 60 frames per second. It implies that the longer period per section, the better the resolution. At the same time, however, the user has to wait a longer time until the first pulse value is presented, which also implies that the possibilities to fast track changes in HR. In this trade-of, for the following computations, sections of 5 seconds length have been used since it can maximally give an estimated pulse that deviates 1 bpm from the true computed value.

5.5.2 Sampling methods

Using *Sampling Method 1*, as defined in section 4.4, did not give as evenly sampled frames as intended. As can be seen in figure 15, the time between two processed

images was not exactly 0.05 s, but turned out to deviate around this number. Since it is of much value for following processing that the signal was evenly sampled, *Sampling Method 1* has not been used for succeeding computations. Instead, *Sampling Method 2*, using interpolation as presented in section 4.4, had been chosen for the purpose of our program.

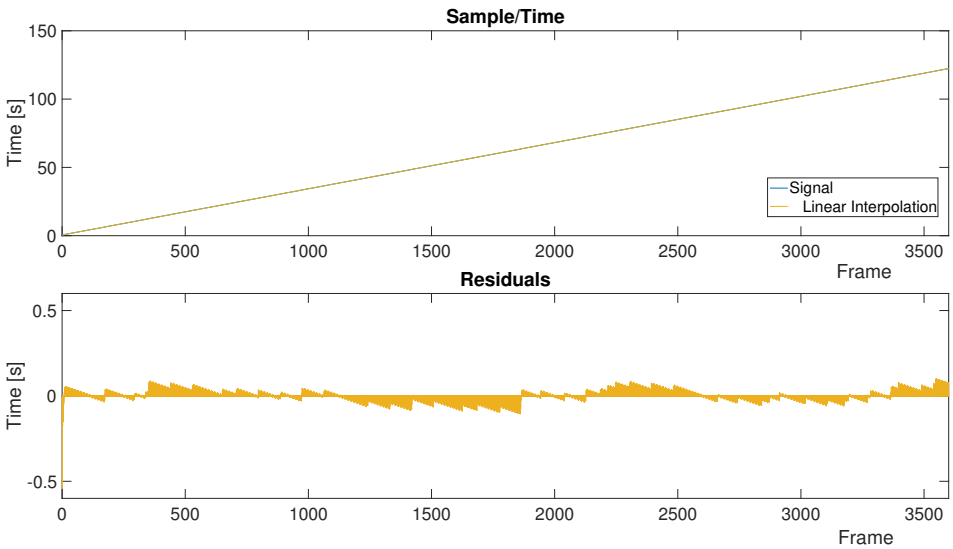

Figure 15: Time stamps of taken frames, compared to a linear plot showing the inherent time difference

Using linear interpolation, according to *Sampling Method 2* has given the results shown in Fig. 16a. It it clear to see in Fig. 16b that the interpolated point appear within the interval of the sampled signal and does not make any extra oscillations.

5.5.3 Zero-padding

In table 5 the results of the two different zero-padding methods can be observed. During this test the settings of the program were such that the total length of values where about 1810. In the case where Welch's method was not used the closest radix using *Zero-padding method 1* was thus 11, which is 2048 (2^{11}). In this case only 238 zeros were added to the vector, according to equation 22. If *Zero-padding method 2* was used it resulted in 2286 zeros (2^{12}).
In the case where Welch's method with 2 sections was used the closest radix was 10, which results in 119 zeros being added to the vector of 905 values, according to *Zero-padding method 1*. If radix 11 instead is used, following *Zero-padding method*

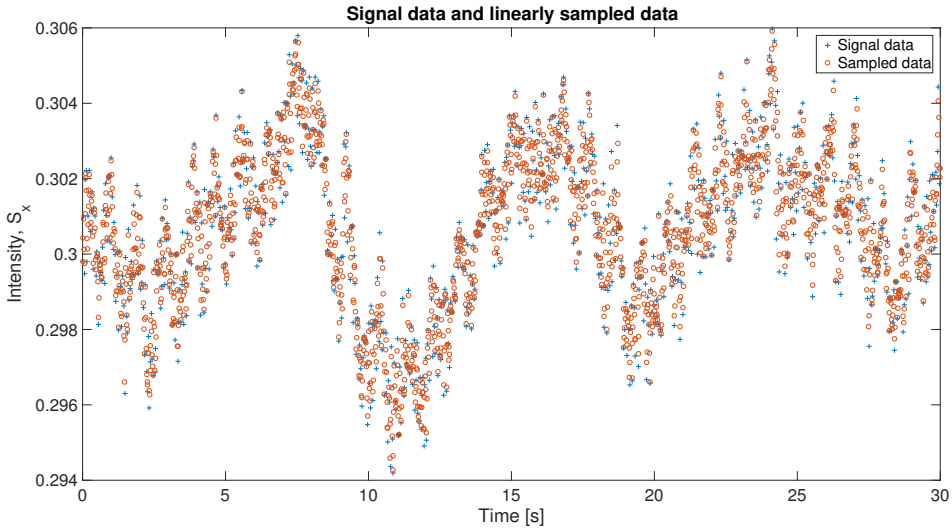

(a) Not magnified

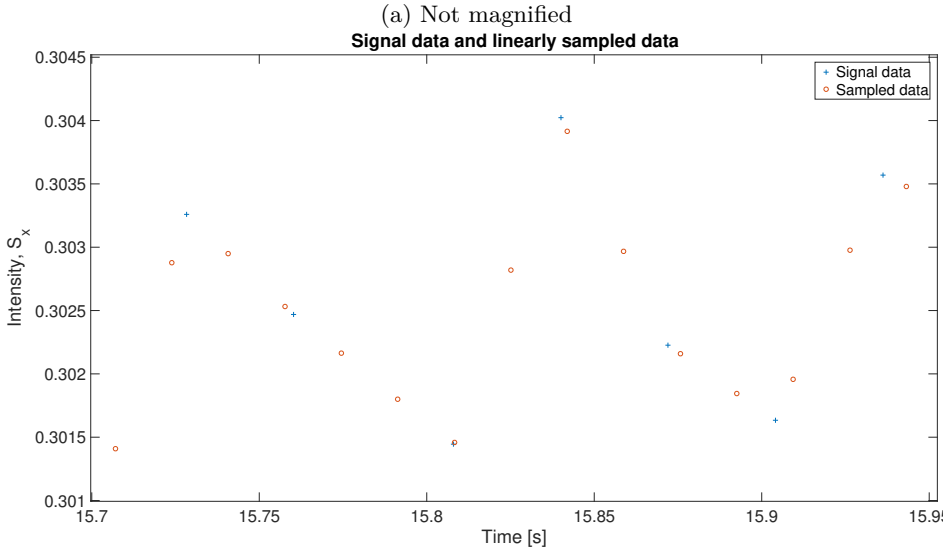

(b) *magnified version of (a)*

Figure 16: *Comparison between in signal data and linearly interpolated data*

2, there is 1143 zeros being added to the vector which again gives a significant increased vector length.
In the case of Welch's method using 4 sections the closest radix is 9, 60 zeros is

thus added to the vector. If a radix of 10 is used 572 zeros are added to the vector.

$$2^x - \frac{\text{Length of vector}}{\text{Number of sections}} = \text{Number of zeros being added} \tag{22}$$

5.5.4 Resolution of frequency spectrum

In Fig. 18a-19b spectrum of a test using different parameters of Welch's method are presented. The test was performed using *ROI method 2*, 6 sections with a time limit of 5 seconds and zero-padding.

Using Welch's method affects the spectral resolution as described in section 3.9. Denoted in Table 5 are the number of units apart different combinations of methods can dissolve. As can be seen, there is no big difference between using and not using *Zero-padding method 1* when it comes to the same Welch's method. However, when *Zero-padding method 2* instead is used, there is a significant amelioration of the spectral resolution. For this reason, *Zero-padding method 1* was left aside in the developed program in advance for *Zero-padding method 2*.
As mentioned in section 5.3 Welch's method has advantages for use on signals with much noise. It does however impair the spectral resolution, and on this cause the developed system originally will run without Welch's method. If the signal is found to be very noise Welch's method can be manually applied. One case where Welch's method was required was the case with test subject A as described in section 5.3. The first few runs of tests were processed without use of Welch's method. This gave a spectrum with much noise and no distinct peak at all, as can be seen in Fig. 17a. Applying Welch's method using 2 segments with 50 percent overlap resulted in the spectrum shown in Fig. 17b. It can be seen comparing the spectrums with and without Welch's method applied that the noise levels are reduced with Welch's method, but there is still no distinct peak at the frequency that corresponded to the pulse measured by ECG.

5.6 Estimated Heart Rate

As presented in Fig. 20a, the first value was in some cases incorrect. In these cases, it was a clear difference between the first and second presented pulse estimation. Despite this the first value was not eliminated in order to not loose valuable information in the cases where it was not deviating much from following values. In order to not affect the succeeding estimation though, 19 was not applied to the first and second estimations, but starts after second presented value.
In Fig. 20b it can be seen that there is a delay between the first and second frame. This was a problem that occurred from time to time, not in all recordings but in many of them, and it has a clear connection to the incorrect first values.

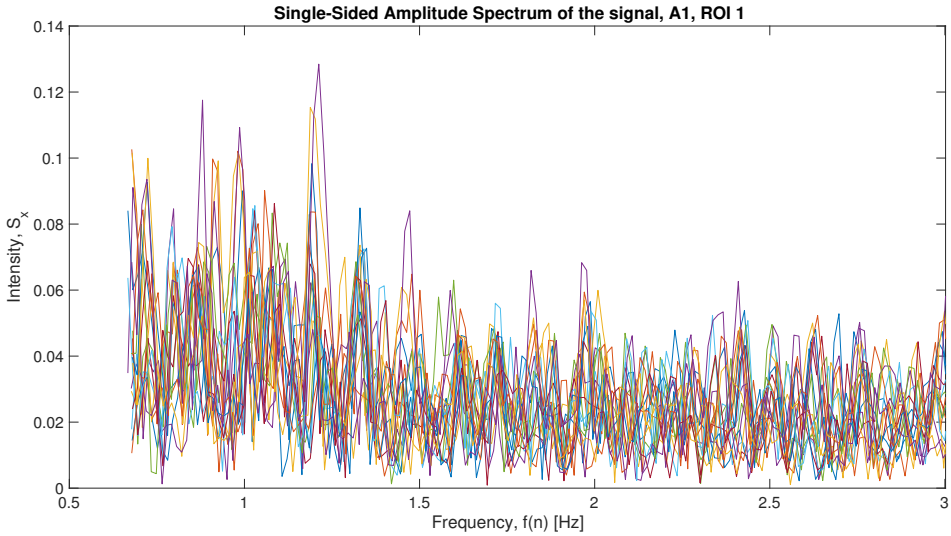

(a) without Welch's method

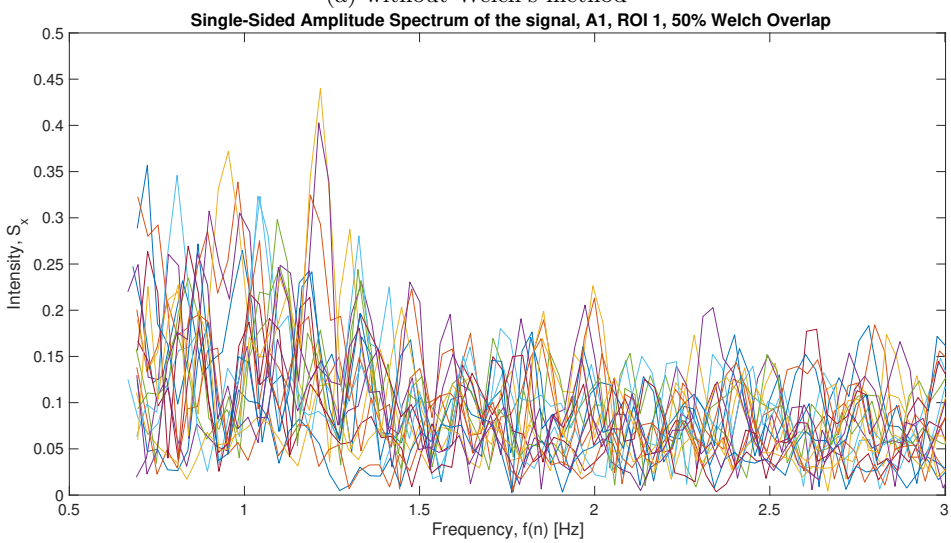

(b) with Welch's method using 2 segments and 50 percent overlap

Figure 17: FFT of signal from test person A, using *ROI method 1*, 6 sections with a time limit of 5 seconds and zero padding.

Zero-padding	Method	ΔR
2^x	No Welch	0.029 Hz
2^x	Welch 2 sections	0.058 Hz
2^x	Welch 4 sections	0.117 Hz
2^{x+1}	No Welch	0.015 Hz
2^{x+1}	Welch 2 sections	0.03 Hz
2^{x+1}	Welch 4 sections	0.059 Hz
No	No Welch	0.033 Hz
No	Welch 2 sections	0.066 Hz
No	Welch 4 sections	0.133 Hz

Table 5: Spectral resolution, ΔR, as presented in section 3.9, using varying combinations of methods

5.7 Segmentation parameters

Since the spectral resolution should be maintained, the main difference of a larger window size and a smaller number of segments would be that the user would have to wait longer for the results. In the final code, 6 segments were chosen, since it allows the system to update once about every 5:th second. This allows for fast readouts, after the initial segments have been filled.

5.8 Performance of the developed program

From table 6 it can be observed that the computational part of the code takes about 0.1 seconds. The data is presented as the mean and standard deviation of 19 test for each of the parameter sets. The calculations are presented in section 3.10. No distinct differences can be noted between the varying methods, since the small variations can also be due to other processes running at the same time in the computer. This means that 3 frames would be lost at every processing cycle if the camera captures with a frame rate of 30 fps and no parallelism is occurring.

5.8.1 Tracking changes in HR

During one of the tests, the subject had a fast rising pulse followed by a fast lowering again. This is demonstrated in Fig. 21. It can be seen that between 55 seconds an 60 seconds in to the recording, the subject's pulse varied from 66.5 bpm to 72.1 bpm. 5 seconds later, the peak corresponding to 72.1 bpm was again reduced to an amplitude lower than the amplitude of the peak at 66.5 bpm. Demonstrated by this example, is that the developed system is able to detect these fast changes.

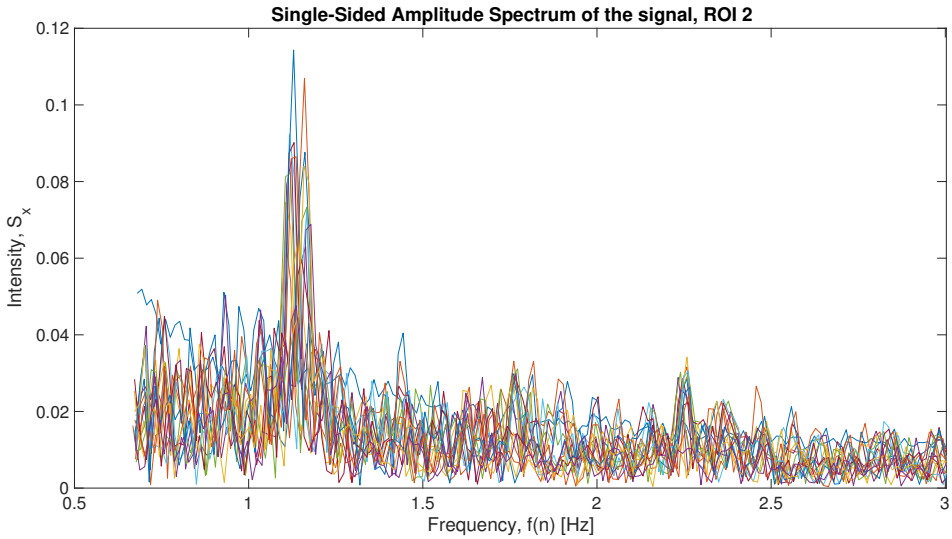

(a) Spectrum when not using Welch's method

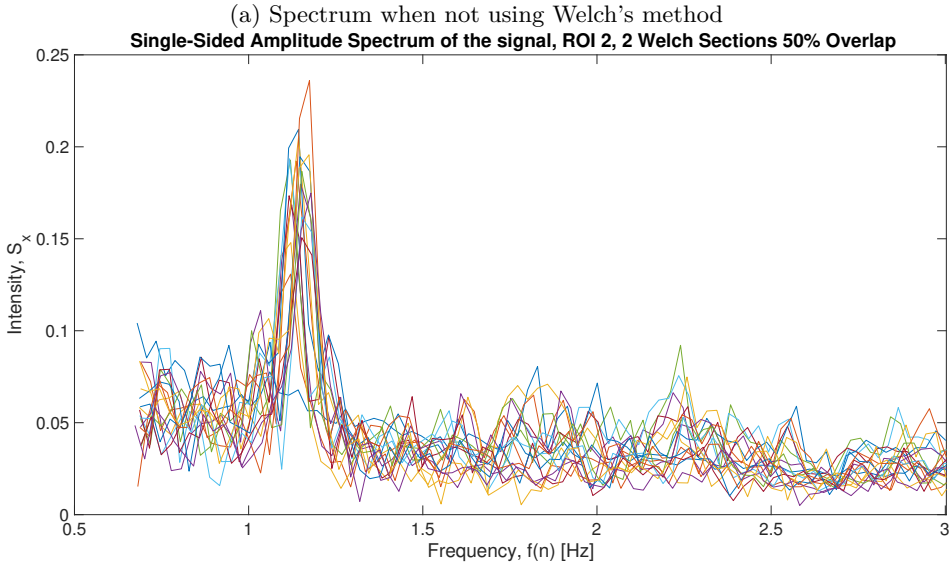

(b) Spectrum when using Welch's method with 2 sections and 50 percent overlap

Figure 18: *Comparison between not using Welch's method and using it with 2 sections with 50% overlap*

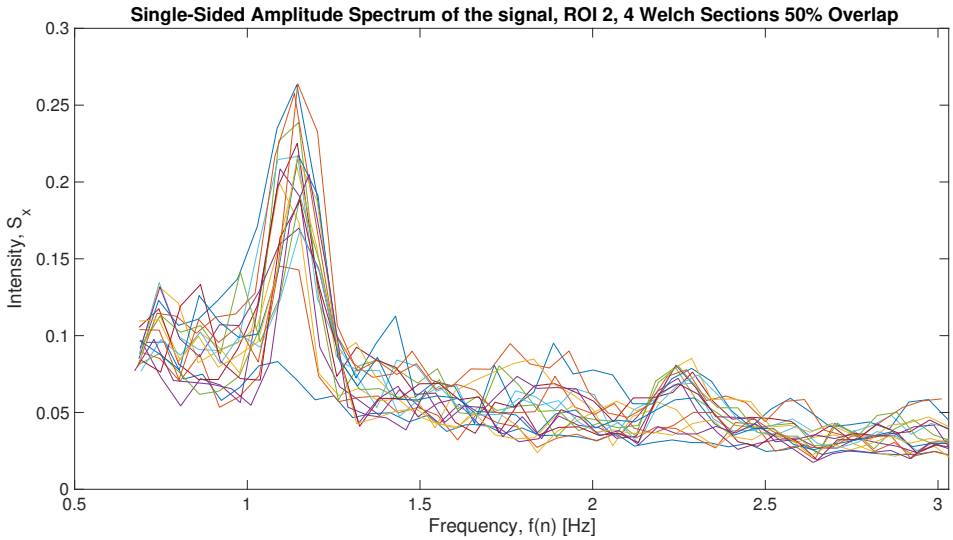

(a) Spectrum when using Welch's method with 4 sections and 50 percent overlap

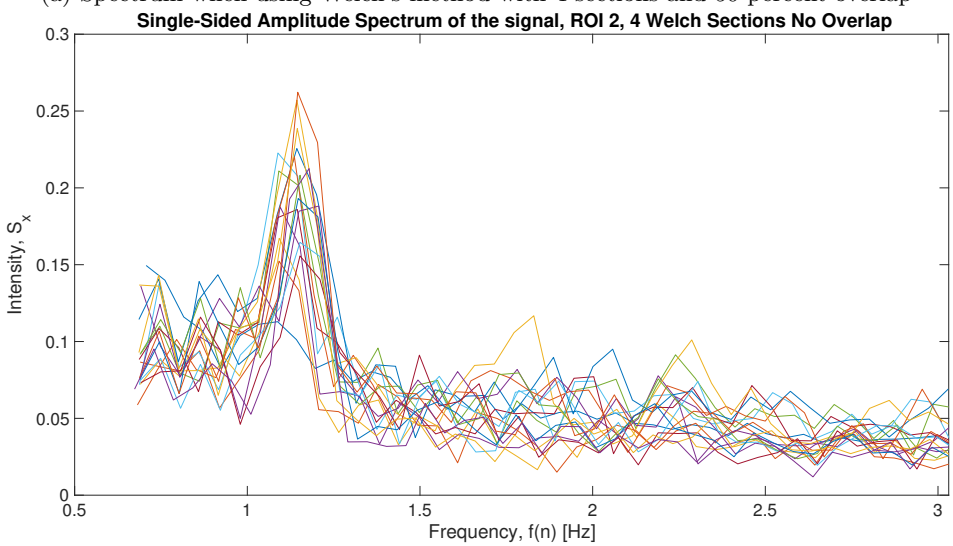

(b) Spectrum when using Welch's method with 4 sections and no overlap

Figure 19: *Comparing usage of Welch's method with 4 sections and varying amounts of overlap*

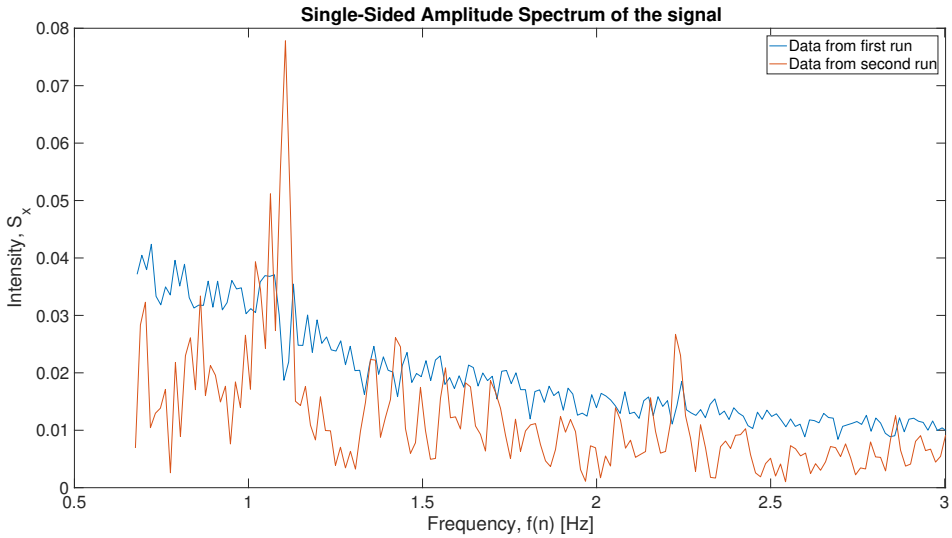

(a) Spectrum with the first two results presented

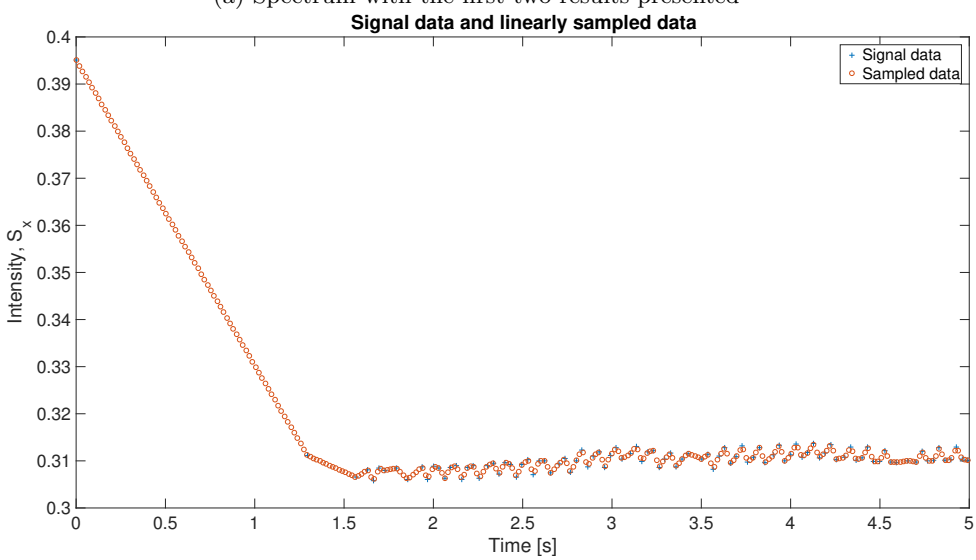

(b) Start up problems and a comparison between in signal data and linearly interpolated data

Figure 20: Start up problems arising from recording

Zero-padding	Method	Elapsed time [s] Mean ± std dev	Comp time [s] Mean ± std dev
2^x	No Welch	0.1021 ±0.0158	0.1059 ±0.0212
2^x	Welch 2 sections	0.1021 ±0.0152	0.1103 ±0.0199
2^x	Welch 2 sections 50 Percent overlap	0.1023 ±0.0135	0.1051 ±0.0181
2^x	Welch 4 sections	0.1002 ±0.0132	0.1016 ±0.0162
2^{x+1}	No Welch	0.0978 ±0.0108	0.0990 ±0.0113
2^{x+1}	Welch 2 sections	0.0998 ±0.0118	0.1025 ±0.0162
2^{x+1}	Welch 2 sections 50 Percent overlap	0.1002 ±0.0116	0.1042 ±0.0175
2^{x+1}	Welch 4 sections	0.0994 ±0.0131	0.1016 ±0.0145
No	No Welch	0.0979 ±0.0104	0.1016 ±0.0136
No	Welch 2 sections	0.0998 ±0.0116	0.0990 ±0.0143
No	Welch 2 sections 50 Percent overlap	0.0998 ±0.0113	0.1068 ±0.0170
No	Welch 4 sections	0.0993 ±0.0119	0.0990 ±0.0143

Table 6: Mean value and standard deviations of timing data calculated from 19 tests using different methods

5.8.2 Statistical Analysis

Estimations of the difference between the reference and estimated pulse are presented in Table 3. The equations used for calculations are presented in section 3.10.

$$\Delta^* = 0.47 \tag{23}$$

$$\sigma^* = 1.30 \tag{24}$$

In (24) an estimation of the standard deviation of the mean value is presented. In (25) a 99% confidence test can be observed.

$$I_\delta = [0.05, 0.89] \tag{25}$$

Following these results, the mean value of deviation from the performed measurements is approximately 0.47. Given the total performance of the developed system, the estimated mean value is with 99% significance within the interval of approximately 0.05 to 0.89 bpm over the reference heart rate measured by ECG. These results shows that there is a statistical difference between the methods using

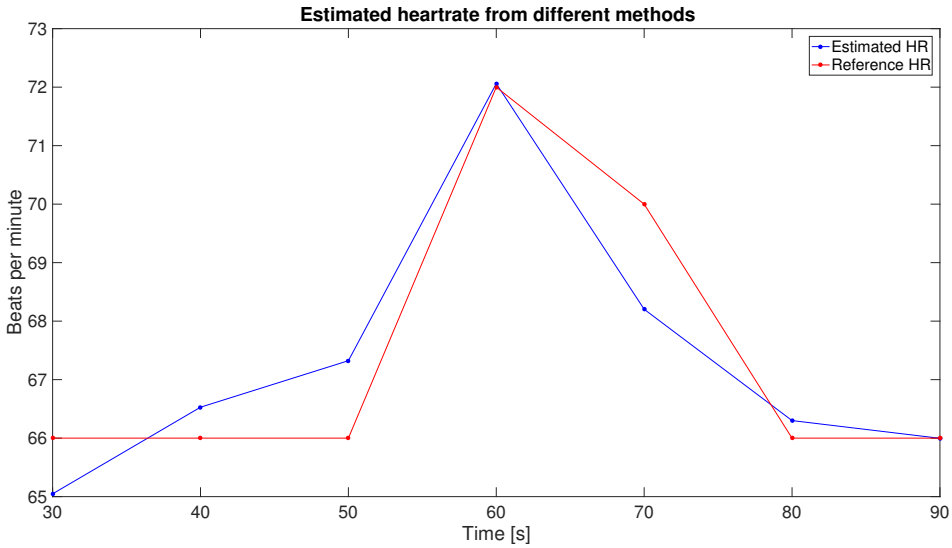

Figure 21: Difference between estimated HR and reference HR in tracking fast changes of HR

this dataset.

5.8.3 Outlier rejection

There is one point that distinctly deviates from the others. This result was given during the testings in the noise-inducing localization for person A, as described in section 5.3. If this outlier was to be rejected, the results would instead be as shown in (26) to (28). These results shows that even if the outlier was removed there still would be a statistical difference between the methods.

$$\Delta^* = 0.40 \tag{26}$$

$$\sigma^* = 1.17 \tag{27}$$

$$I_\delta = [0.02, 0.78] \tag{28}$$

5.9 Graphical user interface

In order for the user to have a simple way to start the measurements an application in MatLab has been suggested, as can be seen in Fig. 22. If the user only presses the button *Start measurement* it is started with the optimized settings as presented in this report. Since the aim was to have an easy-to-use system there are not many possible choices to make for the user. If the user has anything covering the forehead, he/she is encouraged to change ROI method. It is also encouraged to apply Welch's method if problems with a noisy signal are encountered.

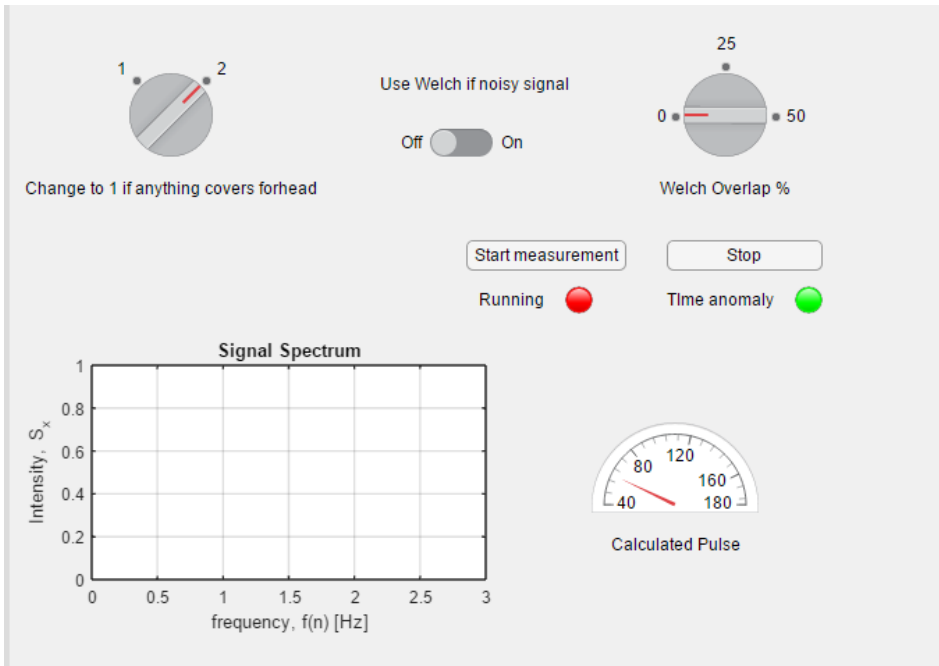

Figure 22: The interface of the application as presented to the user

6 Discussion

The results from the statistical analysis showed that there is a statistical difference between the pulse estimated by the developed program and the reference pulse. The ECG reading were slightly less than half a beat higher than the output of the system. Based on the resolution used during the testing, this kind of difference was expected. It was however expected that about as many values would be below as over the reference which would have made this effect cancel out. To be able to draw a conclusion on why this effect occurs, more tests would have to be performed. One alternative is that it would show that the system would always give an estimated value of half a beat lower than the reference, and it might thereafter be possible to either find the reason or add a variable which increases the value of the mean difference to every result presented. Another option is that after performing many more tests a relationship between deviation and subjects of a certain skin color, ages, environmental factors etcetera could be found. Then it might be possible to design parameters matched with the ruling circumstances to obtain a more correct pulse estimation.

In Table 3 the deviation from the expected value is shown along with the average deviation from the expected value for each test in the last column. From this data it can be observed that there is a large difference in deviation between the tests. This is likely due to the different environments in which the tests where conducted. As explained in the section 5.3, test A_1 had a high number of sources for noise. Since the same person A was tested on in different environments without this blurry result, it seems likely that the problem in this case was the surroundings. On the other hand, no further testings were performed in the noise-inducing location so there might have been other problems disturbing the signal in the recordings. For example, it was noticed that the subject wrinkled his forehead many times. Repeating this behaviour did thought not give any similar results, whether with the same or other subjects. As can be seen in Table 3, when changing the location for person A, just minutes after the first recording was done, gave much less average of deviation.

Given the assumption that was made that the light intensity was to be constant throughout the recordings, this meant a risk for many possible noise sources. As mentioned in section 5.1, one test was cancelled out because it was disturbed by light variations from a drape moving from the window which let in a little more light. There are many possible cases that we had to watch out for in our recordings, such as having a tablet or phone light up in front of the subject, or somebody walking past the light source shadowing the subject. An easy solution for this problem could be to have a white paper with a black cross on it taped on the wall next to the subject. If the program was designed to set the light intensity due to the intensity changes on the paper, under the assumption that the intensity at the paper and at the subject are linearly dependent, this would make the system much

more robust.
In Fig. 13a, 13b and 13c the different locations of performed tests can be observed. Despite our belief that the location had a strong input on the deviation, no clear connection can be seen between the tests performed in the same surroundings. This is probably due to the varying amounts of light coming from the window since the sunlight could not be completely blocked out. The tests were performed on different times of the day as well as with different weather which made the amount and intensity of sunlight vary much even though the locations of several tests were the same. The system takes into account the amount of light at the beginning of the recordings, but for example if the sun is shadowed this would cause alterations in the light intensity through the window.
For future testings, we would suggest using a room without windows and the light source placed in front of a fixed location from the subjects. Nevertheless, the aim of the project was to construct a system that worked well without having to take in to consideration all parts of lighting sources and intensities. On this basis, performing the tests in an optimal environment allows for the system to be optimized in good conditions first. It would then be easier to draw conclusions on how the system is affected in different more challenging environments and thereafter construct a more robust system. Our theory is that combining the paper taped on the wall, with further testings in a specific test room would allow for much amelioration of the developed system when it comes to robustness of surrounding factors.
The reason of the difference in deviation from the reference value between the individual tests can also be altering types of movements that could not be fully compensated for using the implemented localization and traction of face methods. The movement would thus have to be in the frequency range of interest and of much intensity to have affected the measurements.
As can be seen in Table 5, there is no big difference in resolution of frequency spectrum between not using Welch's method, and using it with 2 sections. Since Zero-padding aims to get the closest 2^x number of L samples in the sequence, it seems likely that the same number of 2^x has been chosen for the two methods. However, when using Welch's method with 4 sections, a bigger difference in resolution can be noticed. This indicates that another radix was used.
Another aspect that can be observed in Table 5, is that there is a big difference in the distance between data points in different types of zero padding. At the same time the difference is not as big between the distance between data points in zero padding to the closest radix compared to not using zero padding. This is most likely due to the data being close to a radix and thus not so many values are added to the vector. If the data would have been further apart from the radix the difference of using zero padding compared to not using it would have been much larger.
As this system is designed to be used with different vector configurations we believe

that it is preferable to always increase the vector by one extra radix instead of hoping that the length will be appropriate. Of course there could be a statement to check if this is the case and add the radix in case the values where too close to a radix but based on the small difference in elapsed time between the methods, as presented in Table 6, this was not considered to be necessary.
During several of the tests, time anomalies occurred in the program. This caused a delay between some samples. In section 5.6, our solution to this problem is presented. Using the live version of the program, this will thus not cause any problems. Nonetheless, in the recorded videos this delay between samples still exists, meaning that some beats may have been lost between spaces. Given our presented solution, it will not give misguiding pulse estimations, but gives no output during this delay.
The time anomalies are most likely due to Microsoft Window's processes running in the background of the operating system and Matlab not being prioritized. This might be solved by running the program on another operating system or setting it as an priority.
The application connected to the program was designed in order for the user to get easily started without having to understand the background of the system. It was considered to be better to leave many choices out instead of risking to confuse the user with many different alternatives, and therefor only two cases of options are possible. The application could however benefit from further development concerning the design to make it a more appealing and intuitive user interface.
As mentioned in section 4.5, the first value is miss guiding in many cases. The reason for this is that there is a start up delay in the used camera. This delay induces long times between taken frames in the beginning of the recordings, which makes it possible that one or several heart beats are missed between frames making the estimated pulse incorrect. Despite this, we have chosen not to remove the first value presented since it is not always wrong, and if rejected despite a correct value, significant data might be lost. In the cases where it is incorrect, this is clearly visible given the difference that then occurs to the following presented pulse 5 seconds later on in the process. Therefor it is easy to disregard the first value if it is clearly incorrect even thought it is presented to the user. This problem made us implement a safeguard as the first result is not kept as a reference value for the following results.
We found it very interesting that the *ROI method 2* where measurements were only performed on the forehead actually gave better results than *ROI method 1* which measures on the whole face. It turned out that at the same time as the pulse signal strength increased, so did the noise to an even larger extent. The *ROI method 2* thereby gave better results with less noise. As mentioned in section 4.3 the areas with highest density of blood vessels in the face are the cheeks and the forehead. When increasing the region of interest to a 60 percent width of the face

large parts of the cheeks are included, but so are the eyes, the nose and the mouth. These part does not contribute with as much information about the heart rate but instead are extended areas for noise inducement, which is probably why the signal to noise ratio is reduced. Eye movement are not accounted for in any of the applied algorithms, and thus it can be a major fault source when the movements are within the chosen frequency range.
Using the different equations for validating that the found peak actually corresponds to the heart rate is essential for a good estimation. The equations and their parameters have been developed after localization of errors during the testing. Using the parameter values as defined in (18), (19) and (20) seems to give good results but they can of course be a reason for certain cases of deviation from the reference pulse.
In the beginning of the process, some problems were encountered that the program chose values that actually not corresponded to a true peak, but were the first high value on the down going slope of a peak that was outside of the interval. It was therefor assumed to be part of noise. To assure that a peak was chosen, avoiding this situation, equation (18) was introduced.
As was presented in Fig. 21, there was one case where the pulse acquired from the system varied 8.76 bpm in only 5 seconds. This was the only observed case detecting as fast of a change of pulse, and therefor the limit of equation 19 was set to 10 bpm during 5 seconds. It was crucial that the true fast changes was not to be removed by this limit, but at the same time a limit set too high would increase the risk of detecting the wrong peak as estimated pulse.
Equation (20) were introduced to make sure that the chosen peak was significantly higher than the rest of the signal. It is a combination of two validating test to assure both that the estimated pulse is distinct and that good information should not be thrown away too easily. In this trade-of between accurate estimations and giving an output from the section in question, the limits of 10 respectively 120 percent were chosen by empirical research.

Many of the methods and algorithms presented in the theory section of this report have not been implemented, for example applying different filters. Filters were not found to be necessary since the signal was transferred to frequency domain using FFT, and then only analyzing the frequencies between 40 and 240 bpm. It would however have been interesting to compare our method to methods including joint time-frequency analysis and heuristic methods for extraction of pulse signal. It would also have been interesting to try different combinations of color channels, instead of only extracting the green channel. The applied methods, however, have been chosen with consideration taken to the time limit of this project and the method's capacity to work good in the developed program.

6.1 Ethics

When looking at what the future might bring using the presented technique, there are several ethical questions that can be raised . First of all, during the development of this technique, tests have to be performed on many persons. Of course, it is then the biggest priority to make sure that the participation is completely voluntarily and that the subjects are aware of the process of the test. Beside that, if any information about the subjects are to be presented, the subjects have to be informed and give their approval. In this report, the subjects personal information, such as names and ages, has been substituted by simply a letter A-I. However, a photo of one of the subjects has been included in the report, of course with the consent of the subject himself.

In a yet further perspective in a cradle to grave perspective is the usage of this technique. In hospital care, we do not find many troublesome situations since the method only adds up to other monitoring and measuring products, but for monitoring people in their homes the case is another.

According to Johansson, [36] there are four major biomedical ethical principles that have to be considered during the development of such technique:

- Autonomy, respecting the self-determination and allow people to make informed choices.
- Justice, such as distributing advantages, disadvantages, risks and costs fairly. Distributing resources, conquering needs, rights, obligations and so on.
- Beneficence, meaning that the intentions are good
- That it may not harm, which demands that the connection between cause and harm is avoided, saving both the patient and others from harm. If the procedure would encounter any harm it is important that it is not disproportionate compared to the advantages of the method.

In order to fully respect the autonomy we consider it very important that the patient may disagree to usage not only when the method is introduced but at all times. For the sake of making an informed choice, this might for example include that a lamp is implying if the camera is recording and that the patient has the possibility to turn the measurements of at any time. How exactly this would be implemented when it comes to alarming the system when it is not recording or if the person is not of full mental health would have to be further explored.

Another question we would like to raise is if the system could be hacked, giving the information to a third party. Before introducing this technique there would have to be much investigations into this field to assure that the information is collected and stored safely and may not be obtained or altered by anyone not granted access.

We do believe that usage of this technique, if correctly implemented, could give many benefits to future patients in their homes. The integrity would have to be investigated in each individual case, when it comes to the trade of between recording in ones home at the same time as the possible visits from caretakers or

going to the hospital might be reduced.
To summarize, the field would have to be further explored before introducing this technique, but looking at other recording or monitoring devices being used in health care, we believe that the benefits of this technique in many cases would overcome the possible disadvantages.

7 Conclusions

Despite the limited time, it has been possible to construct a fairly robust system. Problems using the system have been encountered when there were several light sources from different angles and when the light intensity was not stable. The conclusion could thus be drawn that from where the light emerged and the variation of the light was more important then what type of light source was used.
Tests have been performed in different environments on 9 persons of varying ethnicities, ages and genders. Calculating a mean value for the difference between the pulse estimated by the developed program and the reference ECG measurements, 99% of the mean difference fell within approximately 0.05 and 0.89 beats per minute (bpm) over the reference. The mean value of the performed test were approximately 0.5 bpm. This means that there is a statistical difference between the pulse estimated by the program and the reference pulse.
The developed program is compatible with many different simple digital cameras and require no specific light source. It is also easy to execute measurements for the user. On this basis, our strong belief is that with further tests and adaptations of the program, the method presented can be of much value in the health care of the future.

8 References

References

[1] Yu Sun and Nitish Takor,*Photoplethysmography Revisited: From Contact to Noncontact, From Point to Imaging*, IEEE Transactions on Biomedical Engineering, vol. 63, no. 3, pp. 463-477, 2016.

[2] Karim Alghoul, Saeed Alharthi and Hussein Al Osman, *Heart Rate Variability Extraction From Videos Signals: ICA vs. EVM Comparison*, IEEE Access, vol. 5, pp. 4711-4719, 2016.

[3] Å. Rustand, *Ambient-light photoplethysmography: How can I tell your pulse from looking at your face?*, Ph.D. dissertation, Norwegian University of Science and Technology, 2012.

[4] D. McDuff, S. Gontarek and R. Picard, *Remote measurement of cognitive stress via heart rate variability*, in proceedings of the 36th annual international conference IEEE Engineering in medicine and biology society (EMBC), pp. 2957–2960, 2014.

[5] S. Tominaga, *Dichromatic reflection models for a variety of materials*, COLOR Res. Appl., vol. 19, pp. 277-285, 1994.

[6] A. B. Hertzman, *The blood supply of various skin areas as estimated by the photoelectric plethysmograph*, Amer. J. Physiol., vol. 124, no. 2, pp. 328-340, 1938.

[7] O. W. Van Assendelft, *Spectrophotometry of Haemoglobin Derivatives*, Springfield, 1970.

[8] J. Lee, K. Matsumura, P. Rolfe T. Yamakoshi, N. Tanaka, K. Kim, and K. Yamakoshi, *Validation of normalized pulse volume in the outer ear as a simple measure of sympathetic activity using warm and cold pressor tests: towards applications in ambulatory monitoring*, Physiol. Meas., vol. 34, pp. 359–379, 2013.

[9] M.-Z. Poh, D. J. McDuff, and R. W. Picard, *Non-contact, automated cardiac pulse measurements using video imaging and blind source separation*, Optics Express, vol. 18, no. 10, pp. 10762-10774, 2010.

[10] M.-Z. Poh, D. J. McDuff, and R. W. Picard, *Advancements in noncontact, multiparameter physiological measurements using a webcam*, IEEE Transactions on Biomedical Engineering, vol. 58, no. 1, pp. 7–11, 2011.

[11] A. R. Guazzi, M. Villarroel, J. Jorge, J. Daly, M. C. Frise, P. A. Robbins, and L. Tarassenko, *Non-contact measurement of oxygen saturation with an rgb camera*, Biomedical optics express, vol. 6, no. 9, pp. 3320–3338, 2015.

[12] E. Jonathan and M. J. Leahy, *Cellular phone-based photoplethysmographic imaging*, J. Biophoton., vol. 4, no. 5, pp. 293–296, 2011.

[13] Yu Sun, Charlotte Papin, Vicente Azorin-Peris, Roy Kalawsky, Stephen Greenwald and Sijung Hu, *Use of ambient light in remote photoplethysmographic systems: comparison between a high-performance camera and a low-cost webcam*, Journal of Biomedical Optics, Vol. 17 (3), pp. 037005, 2012.

[14] W. Verkruysse, L. O. Svaasand and J.S. Nelson, *Remote plethysmographic imaging using ambient light*, Opt. Exp., vol. 16, no. 26, pp. 21434–21445, 2008.

[15] D. McDuff, S. Gontarek, and R. W. Picard, *Improvements in remote cardiopulmonary measurement using a five band digital camera*, IEEE Trans. Biomed. Eng., vol. 61, no. 10, pp. 2593-2601, 2014.

[16] R. R. Fletcher, D. Chamberlain, N. Paggi, and X. Deng, *Implementation of Smart Phone Video Plethysmography and Dependence on Lighting Parameters*, Conf. Proc. IEEE Eng. Med. Biol. Soc., 2015.

[17] P. Viola and M. Jones, *Rapid object detection using a boosted cascade of simple features*, in Computer Vision and Pattern Recognition, 2001. CVPR 2001. Proceedings of the 2001 IEEE Computer Society Conference on., IEEE, vol. 1. , pp. I–511, 2001.

[18] L. Feng, L.M. Po, X. Xu, Y. Li and R. Ma, *Motion-resistant remote imaging photoplethysmography based on the optical properties of skin*, IEEE Transactions on Circuits and Systems for Video Technology, vol. 25, no. 5, pp. 879–891, 2015.

[19] D. E. King, *Dlib-ml: A machine learning toolkit*, Journal of Machine Learning Research, vol. 10, pp. 1755-1758, 2009.

[20] B.-F. Wu, P.-W. Huang, C.-H. Lin, M.-L. Chung, T.-Y. Tsou and Y.-L. Wu, *Motion Resistant Image-Photoplethysmography Based on Spectral Peak Tracking Algorithm*, IEEE Access, vol. 6, pp. 21621-21634.

[21] R. Boda and M. J. P. Priyadarsini, *Face detection and tracking using KLT and Viola Jones*, ARPN Journal of Engineering and Applied Sciences, vol. 11, no. 23, pp. 13472-13475, 2016.

[22] W. Wang, S. Stuijk and G. de Haan, *Exploiting spatial redundancy of image sensor for motion robust rPPG*, IEEE Trans. Biomed. Eng., vol. 62, no. 2, pp. 415–425, 2015.

[23] M. Lewandowska, J. Ruminski, T. Kocejko, and J. Nowak, *Measuring pulse rate with a webcam —A non-contact method for evaluating cardiac activity*, Proc. Federated Conf. Comput. Sci. Inform. Syst., 2011, pp. 405–410.

[24] G. de Haan and V. Jeanne, *Robust pulse rate from chrominance-based RPPG*, IEEE Trans. Biomed. Eng., vol. 60, no. 10, pp. 2878–2886, 2013

[25] B. Ju et al., *Wavelet based measurement on photoplethysmography by smartphone imaging*, Appl. Mech. Mater., vol. 380, pp. 773–777, 2013.

[26] M. Hulsbusch and V. Blazek, *Contactless mapping of rhythmical phenomena in tissue perfusion using PPGI*, Proc. SPIE, vol. 4683, pp. 110–117, 2002.

[27] Y. Hsu, Y. L. Lin and W. Hsu, *Learning-based heart rate detection from remote photoplethysmography features*,Proc. IEEE Int. Conf. Acoust. Speech Signal Process., pp. 4433–4437, 2014.

[28] P. D. Welch, *The use of Fast Fourier Transform for the estimation of power spectra: A method based on time averaging over short, modified periodograms*, IEEE Transactions on Audio and Electroacoustics, vol. 15, no. 2, pp. 70–73, 1967.

[29] G. Blom, J. Enger, G. Englund, J. Grandell, and L. Holst, *Sannolikhetsteori och statistikteori med tillämpningar*, Studentlitteratur AB, 2017.

[30] Mathworks, *MATLAB Support Package for USB Webcams*, Retrieved August 10 20018 from https://se.mathworks.com/matlabcentral/fileexchange/45182-matlab-support-package-for-usb-webcams, Mathworks, 2018

[31] G. I. Taylor and J. H. Palmer, *The vascular territories (angiosomes) of the body: experimental study and clinical applications*, Br J Plast Surg., vol. 40, no. 2, pp. 113-141, 1987.

[32] Daniel J. McDuff, Ethan B. Blackford and Justin R. Estepp, *Fusing partial camera signals for non-contact pulse rate variability measurement*, IEEE Transactions on Biomedical Engineering, in Press

[33] Mathworks, *edfRead*, Retrieved September 5 2018 from https://se.mathworks.com/matlabcentral/fileexchange/31900-edfread, Mathworks, 2018

[34] Mathworks, *Complete Pan Tompkins Implementation ECG QRS detector*, Retrivied September 5 2018 from https://se.mathworks.com/matlabcentral/fileexchange/45840-complete-pan-tompkins-implementation-ecg-qrs-detector, Mathworks, 2018

[35] Intel, *Intel® Core™ i7-7500U Processor*, retrieved October 23 2018 from https://ark.intel.com/products/95451/Intel-Core-i7-7500U-Processor-4M-Cache-up-to-3-50-GHz-, 2018

[36] Lecture by Veronica Johansson, MTh, PhD, LTH, *Neuroethics – an introduction*, February 26 2018, Lunds Tekniska Högskola

9 Appendix

Time vector [s]	**Output System [bpm], no Welch**	**ECG reference [bpm]**
30	72.2724	73
60	67.8004	73
90	65.6959	69
120	71.9041	72

Table 7: Output from system for test A_1

Time vector [s]	**Output System [bpm], no Welch**	**ECG reference [bpm]**
30	66.3710	67
60	67.6690	66
90	69.3505	70
120	70.3186	70

Table 8: Output from system for test A_2

Time vector [s]	**Output System [bpm], no Welch**	**ECG reference [bpm]**
30	61.6024	64
60	61.4607	60
90	-	62
120	58.8659	60

Table 9: Output from system for test B_1 contains a time anomaly at 70 s and 72 s

Time vector [s]	**Output System [bpm], no Welch**	**ECG reference [bpm]**
30	61.6023	64
60	61.5971	62
90	60.5153	60
120	59.6452	58

Table 10: Output from system for test person B_2

Time vector [s]	**Output System [bpm], No Welch**	**ECG reference [bpm]**
30	55.6450	57
60	55.0785	56
90	55.0485	56
120	55.0484	56

Table 11: Output from system for test person C_1

Time vector [s]	**Output System [bpm], no Welch**	**ECG reference [bpm]**
30	56.2875	56
60	55.85	56
90	56.72	56
120	56.3668	56

Table 12: Output from system for test person C_2

Time vector [s]	**Output System [bpm], no Welch**	**ECG reference [bpm]**
30	69.1162	68
60	64.8821	66
90	65.6217	65
120	64.6816	65

Table 13: Output from system for test person D_1

Time vector [s]	Output System [bpm], no Welch	ECG reference [bpm]
30	66.1721	68
60	66.7463	66
90	64.1376	66
120	63.1464	64

Table 14: Output from system for test person D_2

Time vector [s]	Output System [bpm], no Welch	ECG reference [bpm]
30	70.3593	71
60	71.2765	71
90	70.3593	70
120	71.2764	69

Table 15: Output from system for test person E_1

Time vector [s]	Output System [bpm], no Welch	ECG reference [bpm]
30	47.5179	71
60	70.3966	72
90	70.3996	70
120	43.9979	72

Table 16: Output from system for test person E_2

Time vector [s]	Output System [bpm], no Welch	ECG reference [bpm]
30	65.0477	66
60	72.0600	72
90	65.9969	66
120	65.5652	66

Table 17: Output from system for test person F_1

Time vector [s]	Output System [bpm], no Welch	ECG reference [bpm]
30	62.8818	64
60	61.0826	62
90	61.0375	62
120	62.3499	64

Table 18: Output from system for test person F_2

Time vector [s]	Output System [bpm], no Welch	ECG reference [bpm]
30	57.1649	58
60	56.3172	58
90	55.4080	54
120	58.0773	58

Table 19: Output from system for test person G_1

Time vector [s]	Output System [bpm], no Welch	ECG reference [bpm]
30	55.1969	56
60	55.2678	56
90	54.8384	56
120	54.8669	56

Table 20: Output from system for test person G_2

Time vector [s]	Output System [bpm], no Welch	ECG reference [bpm]
30	75.5153	74
60	68.6364	70
90	65.9997	66
120	68.6372	68

Table 21: Output from system for test person H_1

Time vector [s]	**Output System [bpm], no Welch**	**ECG reference [bpm]**
30	72.8809	72
60	73.9166	74
90	70.3595	72
120	71.2769	72

Table 22: Output from system for test person H_2

Time vector [s]	**Output System [bpm], no Welch**	**ECG reference [bpm]**
30	59.1036	58
60	53.6773	54
90	53.6490	54
120	57.0996	58

Table 23: Output from system for test person I_1

Time vector [s]	**Output System [bpm], no Welch**	**ECG reference [bpm]**
30	56.0731	56
60	57.1973	60
90	59.6069	58
120	58.0773	58

Table 24: Output from system for test person I_2